but worsened in ten (11 %). In joints with radiologic improvement, joint destruction (namely, joint-space narrowing), subchondral bone cysts, and erosion were all improved, with marked joint remodeling and improvement in osteoporosis (Figs. 3, 4, 5). The Poznanski score did not change after tocilizumab treatment; however, it was significantly correlated with the total Larsen score ($r = 0.53$, $p < 0.05$).

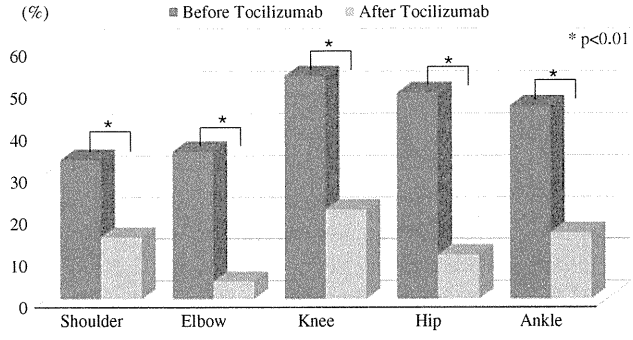

Fig. 2 Frequency of radiologic abnormalities in each joint before and after tocilizumab treatment. In all large joints, the frequency of radiologic abnormalities decreased after tocilizumab treatment

Relative to baseline Larsen grade, all joints at grades III, IV, and V before treatment improved radiologically after tocilizumab treatment. There was one joint at grade 0, seven in grade I, and one in grade II that worsened radiologically after tocilizumab treatment (Fig. 6).

Discussion

Several studies reported retardation of radiologic progression of joint damage after treatment with disease-modifying antirheumatic drugs (DMARDs) or biologics in patients with rheumatoid arthritis (RA) and JIA. Strand et al. [19] reported that monotherapy with methotrexate (MTX) or leflunomide for patients with RA significantly slowed radiologic progression as assessed by total Sharp score, erosion, and joint-space narrowing scores compared with placebo. Regarding the effect of biologics on radiologic progression, RA patients who received etanercept showed significantly less radiologic progression than those receiving MTX, as indicated by the total Sharp score [20]. The Trial of Etanercept and Methotrexate with Radiographic Patient Outcomes (TEMPO) [21] and Anti-Tumour

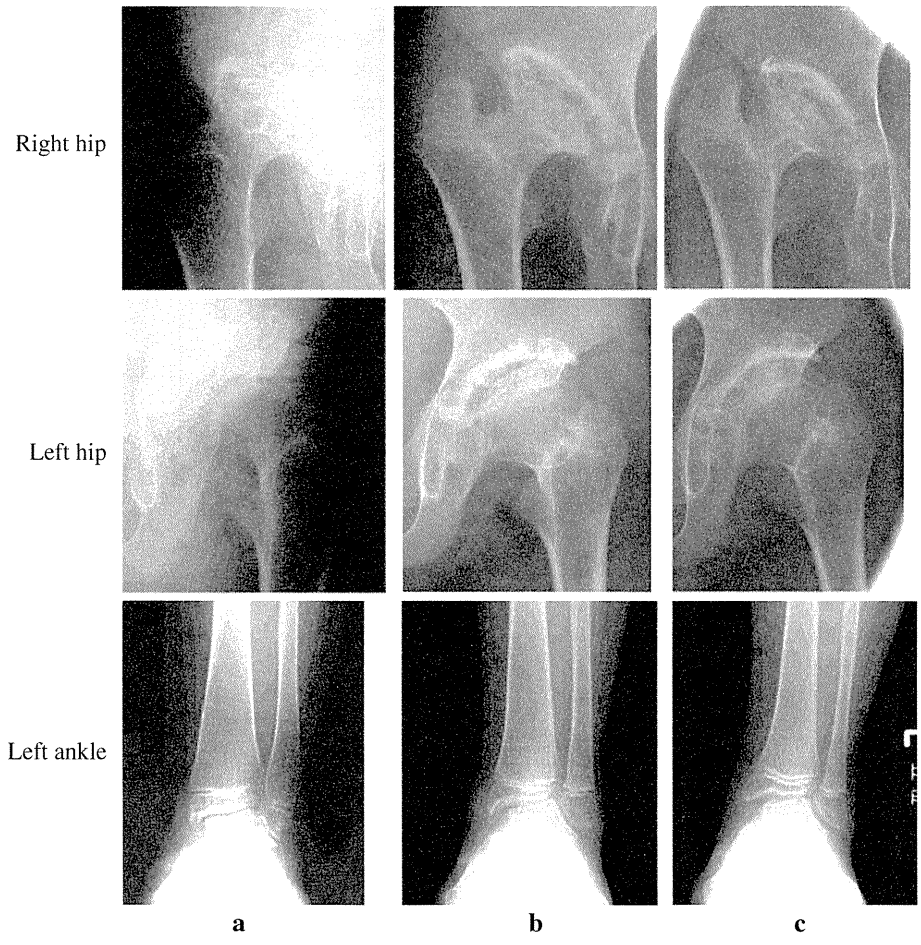

Fig. 3 Improvement in damaged large joints. **a** Before tocilizumab treatment (10.4 years old). Severe erosions, cysts, and joint-space narrowing are observed in bilateral hips. Deformity with marked osteoporosis and joint-space narrowing (1.7 mm) is seen in the left ankle joint. **b** Twenty-eight months after tocilizumab treatment (12.8 years old). Erosions, cysts, joint-space narrowing, and osteoporosis have improved. **c** Fifty-six months after treatment (15 years old). Marked improvement in radiologic abnormalities is observed. Joint-space width of left ankle joint has increased to 2.4 mm

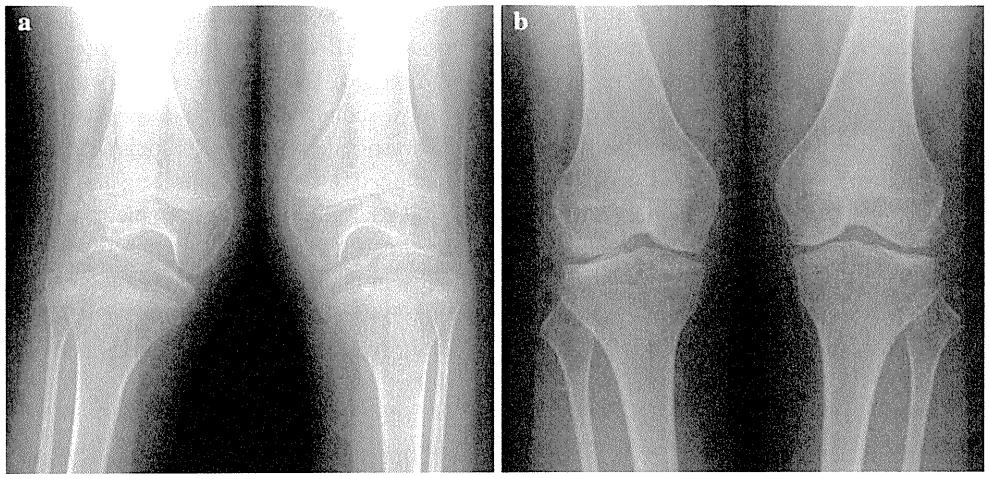

Fig. 4 Improvement in damaged knee joints. **a** Before tocilizumab treatment (9.9 years old). Severe erosions, joint-space narrowing, and epiphyseal irregularity are observed in bilateral knees. Marked osteoporosis is also observed. **b** Erosions and joint-space narrowing are improved, and marked joint remodeling is observed in bilateral knees at 116 months after tocilizumab treatment (19.1 years old)

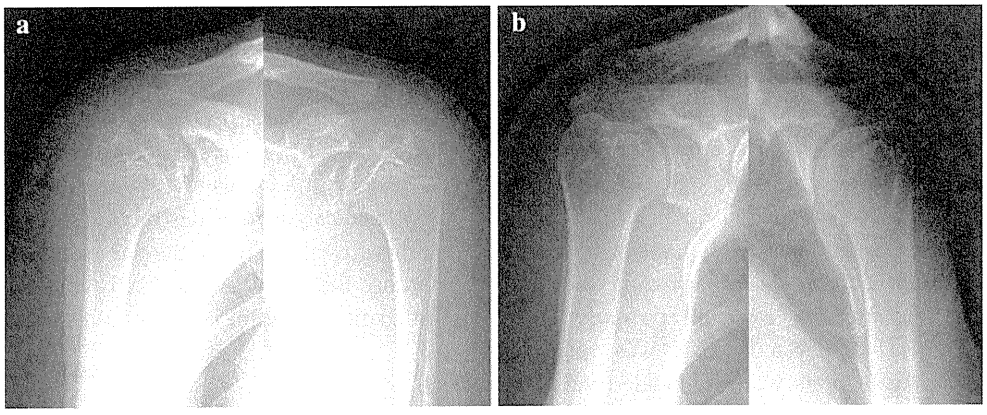

Fig. 5 Improvement in damaged shoulder joints. **a** Before tocilizumab treatment (9.9 years old). Severe erosions, joint-space narrowing, and epiphyseal irregularity are observed in bilateral shoulders. **b** Erosions and joint-space narrowing are improved at 116 months after tocilizumab treatment (19.1 years old); however, localized growth disturbance of the humeral head is observed

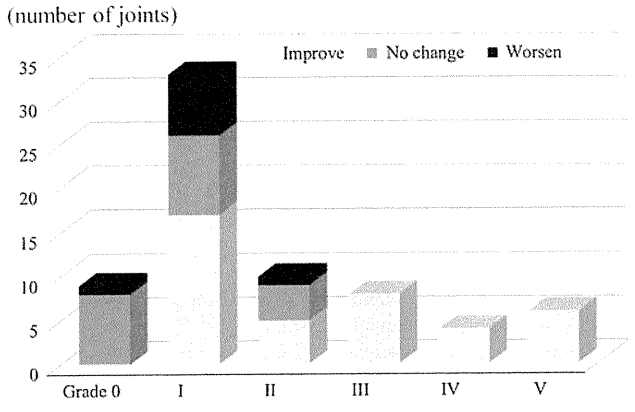

Fig. 6 Baseline Larsen grades and radiologic changes after tocilizumab treatment. In all joints at Larsen grades III, IV, and V, radiologic improvement is observed after tocilizumab treatment. There are also radiologically worsened joints at Larsen grades 0, I, and II (one joint grade 0, seven grade I, one grade II)

Necrosis Factor Trial in Rheumatoid Arthritis with Concomitant Therapy (ATTRACT) studies [22] showed that a combination of etanercept and MTX, or infliximab and MTX, was more effective than MTX or the biological agent alone in retarding joint damage. For patients with JIA, Harel et al. [23] and Ravelli et al. [24] found that MTX was capable of reducing radiologic progression of joint damage. Nielsen et al. [11] reported that the Poznanski score improved after etanercept therapy in children with polyarticular JIA. All these studies used the Poznanski score, the original or modified Sharp score, or the Larsen score for hands, wrists, and feet, for radiologic evaluation, i.e. only the small joints.

Because in childhood the degree of ossification and the width of joint space vary with age, assessment methods for RA are difficult to apply, especially for toddlers. Recent studies have shown that the Poznanski method is a reliable

tool for assessing radiologic progression in patients with JIA [11, 25]. Rossi et al. [26] demonstrated that the Sharp and Larsen methods for the wrist/hand were reliable for assessing radiologic progression in patients with polyarticular JIA, with results similar to the Poznanski score.

Thus far, assessment of joint damage in patients with JIA has mainly been restricted to the small joints of the hands and feet, and there has been no well-established method to evaluate large joint changes radiologically. Pettersson et al. [27] proposed a classification system as a valuable tool for measuring the degree of knee-joint destruction in JIA, which scores osteoporosis, enlargement of the epiphysis, erosion, subchondral cyst formation, and deformed joint surfaces. They demonstrated a good correlation between their classification system and clinical status. For radiologic evaluation of large joints in adult RA, the original or modified Larsen scoring system is used in most studies. In this study, we examined soft-tissue swelling, osteoporosis, joint-space narrowing, epiphyseal irregularity, subchondral bone cysts, erosions, and localized growth disturbance as radiologically abnormal findings in patients with sJIA. We also investigated the frequency of these radiologic abnormalities and the modified Larsen score for radiologic assessment of large joints.

Our study found dramatic radiologic improvement of damaged large joints in several tocilizumab-treated sJIA patients. In those patients, radiologic findings of joint destruction, such as joint-space narrowing, subchondral bone cysts, and erosion, were all decreased after tocilizumab treatment, and osteoporosis was markedly improved. The damaged joints were remodeled very rapidly during treatment and maintained long term. Rau et al. [28] defined radiologic healing characteristics as: (1) reappearance of the cortical plate, (2) partial or complete filling in of an erosion, and (3) subchondral bone sclerosis with osteophyte formation (secondary osteoarthritis). All of these phenomena were seen in the damaged large joints after tocilizumab treatment in our series.

Recent studies show that IL-6 plays an important role in skeletal homeostasis [29, 30]. IL-6 influences both osteoblast and osteoclast activities through a variety of complex mechanisms. Kato et al. [31] reported that receptor activator of nuclear factor kappa-B (NF-κB) ligand (RANKL) was overproduced in arthritis and suppressed by tocilizumab in a collagen-induced monkey arthritis model. They concluded that IL-6 was involved in subchondral bone and bone marrow changes in RA patients. In our study, marked improvement in osteoporosis and bone/joint remodeling occurred after tocilizumab treatment, supporting the role of IL-6 in bone homeostasis.

Seki et al. [32] reported radiologic progression in weight-bearing joints of patients with RA after TNF-blocking therapies and concluded that even in patients with good responses, damaged weight-bearing joints at Larsen grades III and IV showed progression. Additionally, radiologic progression also occurred in less-damaged joints, such as those at Larsen grade I in patients who were nonresponders to TNF blockade. In our study, even in damaged large joints at Larsen grades III, IV, and V, marked radiologic improvement was observed after tocilizumab treatment. Surprisingly, all improved radiologically in our series. This might be a characteristic of JIA in that the regenerative capacity of articular cartilage is better in growing children than in adults [25, 33]. Moreover, damaged joints were remodeled and improvement of radiologic findings maintained for >5 years. To our knowledge, this is the first study to document radiologic improvement and maintenance for long periods after tocilizumab therapy in damaged large joints of sJIA.

However, we note that there were ten joints (11 % of all joints) in which radiologic findings worsened after tocilizumab treatment. There were three patients whose CHAQ was not fully recovered and whose Poznanski score worsened, accounting for most of these progressing joints (seven joints), possibly suggesting that they were less responsive to tocilizumab. Also, we failed to find any improvement in Poznanski scores in this series. This could be because the Poznanski score is unreliable in advanced carpometacarpal joint destruction or on radiologic closure of the growth plate of the second metacarpal bone [34]. Because the study assessed only a small number of cases, further investigation is required to resolve this issue.

Conclusions

Clinical findings and laboratory data confirmed the efficacy of tocilizumab for treating sJIA. Radiologic improvement of the damaged large joints, even the weight-bearing joints, was demonstrated, which certainly improved the quality of life, as shown by the CHAQ results. To our knowledge, this is the first study showing radiologic improvement in damaged large joints in sJIA following biologic therapy. However, damage progression in a minority (11 %) of all joints studied was still observed. Extended studies with larger numbers of cases are required to further establish tocilizumab efficacy.

Conflict of interest Shumpei Yokota received consulting and speaking fees from Chugai Pharmaceutical. Shumpei Yokota and Takako Miyamae is coinventor on a patent for juvenile arthritis treatment. All other authors declare no conflicts of interest.

References

1. Petty RE, Southwood TR, Manners P, Baum J, Glass DN, Goldenberg J, et al. International league of associations for

rheumatology classification of juvenile idiopathic arthritis: second revision, Edomonton, 2001. J Rheumatol. 2004;31:390–2.
2. De Benedetti F, Massa M, Robbioni P, Ravelli A, Burgio GR, Martini A. Correlation of serum interleukin 6 levels with joint involvement and thrombocytosis in systemic juvenile idiopathic arthritis. Arthritis Rheum. 1991;34:1158–63.
3. Mangge H, Kenzian H, Gallistl S, Neuwirth G, Liebmann P, Kaulfersch W, et al. Serum cytokines in juvenile rheumatoid arthritis (JRA). Correlation with conventional inflammatory parameters and clinical subtypes. Arthritis Rheum. 1995;38: 211–20.
4. Quartier P, Taupin P, Bourdeaut F, Lemelle I, Pillet P, Bost M, et al. Efficacy of etanercept for the treatment of juvenile idiopathic arthritis according to the onset type. Arthritis Rheum. 2003;48:1093–101.
5. Gartlehner G, Hansen RA, Jonas BL, Thieda P, Lohr KN. Biologics for the treatment of juvenile idiopathic arthritis: a systematic review and critical analysis of the evidence. Clin Rheumatol. 2008;27:67–76.
6. Woo P, Wilkinson N, Prieur AM, Southwood T, Leone V, Livemore P, et al. Open label phase II trial of single, ascending doses of MRA in Caucasian children with severe systemic juvenile idiopathic arthritis: proof of principle of the efficacy of IL-6 receptor blockade in this type of arthritis and demonstration of prolonged clinical improvement. Arthritis Res Ther. 2005;7: R1281–8.
7. Yokota S, Miyamae T, Imagawa T, Iwata N, Katakura S, Mori M, et al. Therapeutic Efficacy of humanized recombinant anti-interleukin-6 receptor antibody in children with systemic-onset juvenile idiopathic arthritis. Arthritis Rheum. 2005;52:818–25.
8. Yokota S, Imagawa T, Mori M, Miyamae T, Aihara Y, Takei S, et al. Efficacy and safety of tocilizumab in patients with systemic-onset juvenile idiopathic arthritis: a randomized, double-blind, placebo-controlled, withdrawal phase III trial. Lancet. 2008;371: 998–1006.
9. Ilowite N, Porras O, Reiff A, Rudge S, Punaro M, Martin A, et al. Anakinra in the treatment of polyarticular-course juvenile rheumatoid arthritis: safety and preliminary efficacy results of a randomized multicenter study. Clin Rheumatol. 2009;28:129–37.
10. Ruperto N, Quartier P, Wulffraat N, Woo P, Ravelli A, Mouy R, et al. A phase II, multicenter, open-label study evaluating dosing and preliminary safety and efficacy of canakinumab in systemic juvenile idiopathic arthritis with active systemic features. Arthritis Rheum. 2012;64:557–67.
11. Nielsen S, Ruperto N, Gerloni V, Simonini G, Cortis E, Lepore L, et al. Preliminary evidence that etanercept may reduce radiographic progression in juvenile idiopathic arthritis. Clin Exp Rheumatol. 2008;26:688–92.
12. Tse SML, Laxer RM, Babyn PS, Doria AS. Radiologic improvement of juvenile idiopathic arthritis-enthesitis-related arthritis following anti-tumor necrosis factor-α blockade with etanercept. J Rheumatol. 2006;33:1186–8.
13. Inaba Y, Ozawa R, Imagawa T, Mori M, Hara Y, Miyamae T, et al. Radiographic improvement of damaged large joints in children with systemic juvenile idiopathic arthritis following tocilizumab treatment. Ann Rheum Dis. 2011;70:1693–5.
14. Giannini EH, Ruperto N, Ravelli A, Lovell DJ, Felson DT, Martini A. Preliminary definition of improvement in juvenile arthritis. Arthritis Rheum. 1997;40:1202–9.
15. Singh G, Athreya BH, Fries JF, Goldsmith DP. Measurement of health status in children with juvenile rheumatoid arthritis. Arthritis Rheum. 1994;37:1761–9.
16. Larsen A. How to apply Larsen score in evaluating radiographs of rheumatoid arthritis in long-term studies. J Rheumatol. 1995;22: 1974–5.
17. Poznanski AK, Hernandez RJ, Guire KE, Bereza UL, Garn SM. Carpal length in children: a useful measurement in the diagnosis of rheumatoid arthritis and some congenital malformation syndromes. Radiology. 1978;129:661–8.
18. Inamo Y, Harada K. Normal range of carpal length in Japanese children. Nihon Univ J Med. 1998;40:81–7.
19. Strand V, Cohen S, Schiff M, Weaver A, Fleischmann RM, Cannon G, et al. Treatment of active rheumatoid arthritis with leflunomide compared with placebo and methotrexate. Arch Intern Med. 1999;159:2542–50.
20. Genovese MC, Bathon JM, Martin RW, Fleischmann RM, Tesser JR, Schiff MH, et al. Etanercept versus methotrexate in patients with early rheumatoid arthritis: two-year radiographic and clinical outcomes. Arthritis Rheum. 2002;46:1443–50.
21. Klareskog L, van der Heijde D, de Jager JP, Gough A, Kalden J, Malaise M, et al. Therapeutic effect of the combination of etanercept and methotrexate compared with each treatment alone in patients with rheumatoid arthritis: double-blind randomized controlled trial. Lancet. 2004;363:675–81.
22. Lipsky PE, van der Heijde DM, St Clair EW, Furst DE, Breedveld FC, Kalden JR, et al. Infliximab and methotrexate in the treatment of rheumatoid arthritis. N Engl J Med. 2000;343: 1594–602.
23. Harel L, Wagner-weiner L, Poznanski AK, Spencer CH, Ekwo E, Magilavy DB. Effects of methotrexate on radiologic progression in juvenile rheumatoid arthritis. Arthritis Rheum. 1993;36: 1370–4.
24. Ravelli A, Ioseliani M, Norambuena X, Sato J, Pistorio A, Rossi F, et al. Adapted versions of the Sharp/van der Heijde score are reliable and valid for assessment of radiographic progression in juvenile idiopathic arthritis. Arthritis Rheum. 2007;56:3087–95.
25. Poznanski AK, Conway JJ, Shkolink A, Pachman LM. Radiological approaches in the evaluation of joint disease in children. Rheum Dis Clin N Am. 1987;13:57–73.
26. Rossi F, Dia FD, Galipo O, Pistorio A, Valle M, Magni-manzoni S, et al. Use of the Sharp and Larsen scoring methods in the assessment of radiographic progression in juvenile idiopathic arthritis. Arthritis Rheum. 2006;55:717–23.
27. Pettersson H, Rydholm U. Radiologic classification of knee joint destruction in juvenile chronic arthritis. Pediatr Radiol. 1984;14: 419–21.
28. Rau R, Wassenberg S, Herborn G, Perschel WT, Freitag G. Identification of radiologic healing phenomenon in patients with rheumatoid arthritis. J Rheumatol. 2001;28:2608–15.
29. Manolagas SC, Jilka RL. Bone marrow, cytokines, and bone remodeling: emerging insights into the pathophysiology of osteoporosis. N Engl J Med. 1995;332:305–11.
30. Theoleyre S, Wittant Y, Tat SK, Fortun Y, Redini F, Heymann D. The molecular triad OPGRANK/RANKL: involvement in the orchestration of pathophysiological bone remodeling. Cytokine Growth Factor Rev. 2004;15:457–75.
31. Kato A, Matsuo S, Takai H, Uchiyama Y, Mihara M, Suzuki M. Early effects of tocilizumab on bone and bone marrow lesions in a collagen-induced arthritis monkey model. Exp Mol Pathol. 2008;84:262–70.
32. Seki E, Matsushita I, Sugiyama E, Taki H, Shinoda K, Hounoki H, et al. Radiographic progression in weight-bearing joints of patients with rheumatoid arthritis after TNF-blocking therapies. Clin Rheumatol. 2009;28:453–60.
33. Levinson JE, Wallace CA. Dismantling the pyramid. J Rheumatol Suppl. 1992;33:6–10.
34. Magni-manzoni S, Rossi F, Pistorio A, Temporini F, Viola S, Beluffi G, et al. Prognostic factors for radiographic progression, radiographic damage, and disability in juvenile idiopathic arthritis. Arthritis Rheum. 2003;48:3509–17.

Low bone mineral density is associated with the onset of spontaneous osteonecrosis of the knee

Yasushi Akamatsu[1,2], Naoto Mitsugi[1], Takeshi Hayashi[1], Hideo Kobayashi[1], and Tomoyuki Saito[2]

[1]Department of Orthopaedic Surgery, Yokohama City University Medical Center; [2]Department of Orthopaedic Surgery, Yokohama City University School of Medicine, Yokohama City, Kanagawa, Japan.
Correspondence: akamatsu@yokohama-cu.ac.jp
Submitted 11-06-26. Accepted 12-02-20

Background and purpose **The primary event preceding the onset of symptoms in spontaneous osteonecrosis in the medial femoral condyle (SONK) may be a subchondral insufficiency fracture, which may be associated with underlying low bone mineral density (BMD). However, the pathogenesis of SONK is considered to be multifactorial. Women over 60 years of age tend to have higher incidence of SONK and low BMD. We investigated whether there may be an association between low BMD and SONK in women who are more than 60 years old.**

Methods **We compared the BMD of 26 women with SONK within 3 months after the onset of symptoms to that of 26 control women with medial knee osteoarthritis (OA). All the SONK patients had typical clinical presentations and met specified criteria on MRI. The BMDs measured at the lumbar spine, ipsilateral femoral neck, and knee condyles and the ratios of medial condyle BMD to lateral condyle BMD (medial-lateral ratios) in the femur and tibia were compared between the two groups. The medial-lateral ratios were used as parameters for comparisons of the BMDs at both condyles.**

Results **The mean femoral neck, lateral femoral condyle, and lateral tibial condyle BMDs were between x% and y% lower in the SONK patients than in the OA patients ($p < 0.001$). The mean femoral and tibial medial-lateral ratios were statistically significantly higher in the SONK patients than in the OA patients.**

Interpretation **A proportion of women over 60 years of age have low BMD that progresses rapidly after menopause and can precipitate a microfracture. These findings support the subchondral insufficiency fracture theory for the onset of SONK based on low BMD.**

The pathogenesis of spontaneous osteonecrosis of the medial femoral condyle (SONK) remains unclear, although a primary vascular insult and trauma are widely accepted as common causes. However, the pathogenesis of SONK is probably multifactorial (Zanetti et al. 2003, Robertson et al. 2009). Thus, it may be difficult to explain SONK for all ages and both sexes based on a single factor.

Lotke et al. (1977) first suggested a connection between the onset of SONK and subchondral fracture, which was supported by later reports based on MRI and pathological findings (Lecouvet et al. 1998, Yamamoto and Bullough 2000, Takeda et al. 2008). A subchondral insufficiency fracture may result from underlying osteoporosis (Yamamoto and Bullough 2000). This is consistent with a history of sudden onset of pain without a traumatic event (Ahlbäck et al. 1968). In other cases, obesity (Zanetti et al. 2003), overlying degenerative cartilage changes, meniscal tears (Ahlbäck et al. 1968), and meniscal injury (Robertson et al. 2009) may cause increased mechanical loading in the affected condyle, resulting in subchondral fracture.

One study using high-resolution quantitative computed tomography revealed that osteopenia and osteoporosis could be detected in two-thirds of patients with SONK diagnosed by MRI (Zanetti et al. 2003). These observations suggest that some cases of SONK are induced by subchondral insufficiency fracture that may be associated with an underlying low BMD. The incidence of SONK is more common in women than in men, and most of the patients are over 60 years of age (Lotke et al. 1977). A proportion of women older than 60 years have low BMD that progresses rapidly after menopause. Therefore, investigation of women older than 60 years—who may have a common factor—may be useful in clarifying the pathogenesis of SONK. In addition, because previous papers (Houpt et al. 1983, Mears et al. 2009, Robertson et al. 2009) have suggested the presence of preexisting knee osteoarthritis (OA) in patients with SONK, we compared patients with SONK and patients

DOI 10.3109/17453674.2012.684139

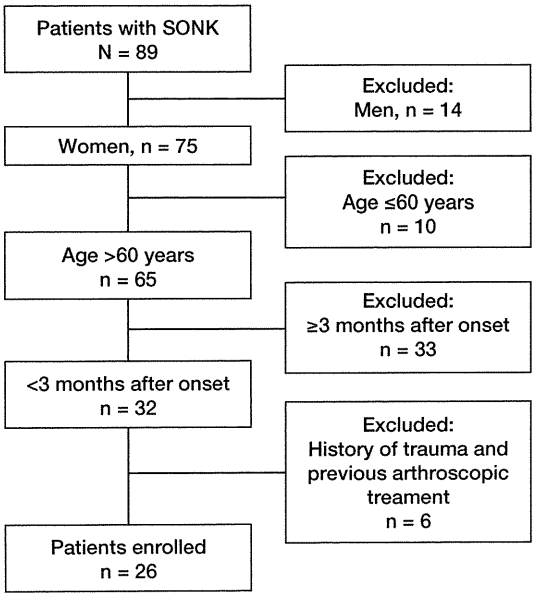

Figure 1. Flow diagram for identifying patients with SONK who were eligible.

with medial knee OA. We assessed the relationship between recent onset of SONK and low BMD at various locations. We also compared the size of lesions by MRI in our SONK patients with those in previous reports.

Patients and methods

Subjects

Between April 2005 and March 2009, we treated 89 consecutive patients with SONK. To target women over 60 years, we excluded 14 men and 10 women who were aged 60 years or less. To minimize the influence of disuse osteoporosis, women with SONK were only enrolled if no more than 3 months had elapsed between the onset of SONK and the time of the BMD measurements. Consequently, of the 65 patients remaining, we excluded 33 women because more than 3 months had elapsed since the onset of symptoms. In addition, we excluded 4 women for having a history of trauma and 2 women for previous arthroscopic treatment. None of the patients with SONK who were included in the study had corticosteroid injections, oral corticosteroid medication, or alcohol abuse. 26 patients remained (Figure 1). All patients were examined by radiography of the knee, knee MRI (Figures 2 and 3), and dual X-ray absorptiometry examinations of the lumbar spine, proximal femur, and knee condyles.

The mean delay between the onset of SONK and its diagnosis based on MRI and BMD measurements was 7 (2–12) weeks. All patients were initially managed nonoperatively. Worsening of knee pain in 15 patients led to surgical treatment mean 17 (6–38) weeks after the initial visit (in 8 patients: high tibial osteotomy; and in 7: a total or unicompartmental knee arthroplasty). Histological sections were obtained from the 15 patients who underwent surgery after a diagnosis of SONK.

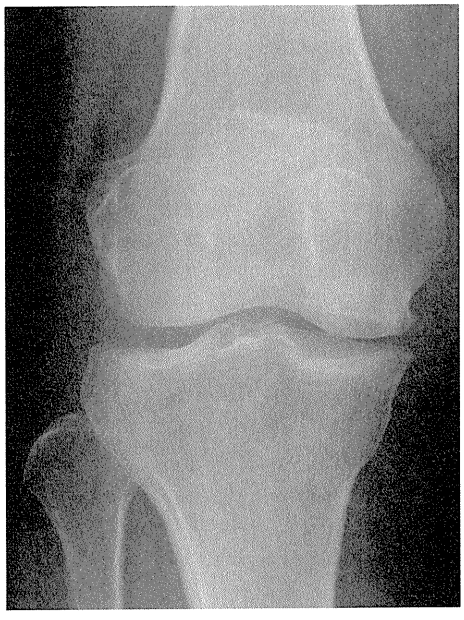

Figure 2. A. An AP radiograph from a 74-year-old woman, who had had sudden onset of right knee pain 7 weeks previously, showing a radiolucent oval lesion in the medial femoral condyle. The patient was classified as being at stage 2 of SONK and Kellgren-Lawrence grade 3.

B. A coronal T2-weighted MRI showed an area of low signal intensity.

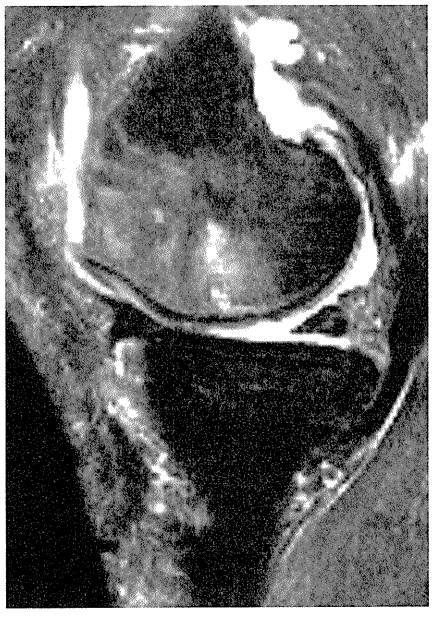

C. A sagittal T2-weighted MRI with fat suppression showed subchondral changes and extensive bone marrow edema.

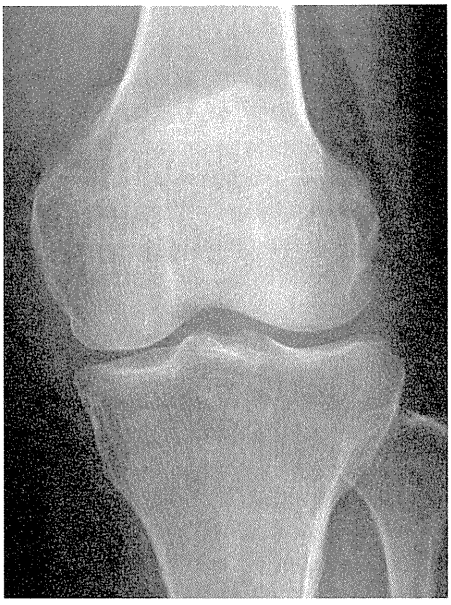

Figure 3. A. An AP radiograph from a 65-year-old woman, who had had sudden onset of left knee pain 10 weeks previously, showing no lesions in the medial femoral condyle. The patient was classified as being at stage 1 of SONK and Kellgren-Lawrence Grade 1.

B. A coronal T2-weighted MRI showed an area of low signal intensity.

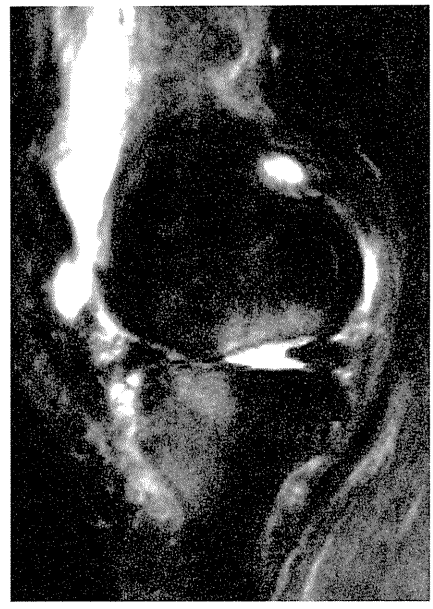

C. A sagittal T2-weighted MRI with fat suppression showed subchondral changes and bone marrow edema.

The diagnoses of the remaining 11 patients were based on the clinical presentation and imaging findings.

The clinical assessment was primarily based on the criteria established by Ahlbäck et al. (1968) and Lotke et al. (1977), comprising sudden onset of severe pain and localized tenderness over the medial femoral condyle.

Previous studies (Houpt et al. 1983, Mears et al. 2009, Robertson et al. 2009) have suggested the potential of preexisting knee OA in patients with SONK. In patients with medial knee OA, varus alignment can serve as a marker of disease severity or progression (Hunter et al. 2007). Thus, we formed a control group of 26 medial knee OA patients who were matched with respect to age, body mass index, and femorotibial angle (the OA group). These patients were considered to have knee OA if they had Kellgren-Lawrence grades (Kellgren and Lawrence 1957) of 2 or higher, and with a medial joint space narrowing of Ahlbäck grade I (Ahlbäck 1968) or lower. Thus, patients with obliteration of the medial joint space were excluded.

The Knee Society knee, pain, and function scores (Insall et al. 1989) were assigned at the first visit.

The study was approved by our institutional review board (number of approval: 1-10-2005-74), and all patients provided informed consent for participation in the study.

Radiography

AP and lateral knee radiographs were taken with the patients standing. Limb alignment was expressed as the femorotibial angle obtained from the AP knee radiograph. The radiograph was also used to determine the stage of progression of SONK, which was classified into 4 stages (Koshino 1982): stage 1, normal radiographic appearance; stage 2, a radiolucent subchondral oval lesion or flattening of the convexity of the condyle, or both; stage 3, expansion of the radiolucent area surrounded by a sclerotic halo and a calcified plate; stage 4, secondary osteoarthritic changes. 6 knees with stage-1 disease had MRI confirmation and, on follow-up, had stage-2 disease or higher on plain radiographs within 1 year of the onset of disease.

MRI

We used a 1.5-T GE Sigma Scanner (General Electric Medical Systems, Milwaukee, WI). Spin-echo pulse sequences were used exclusively for T1-weighted spin-echo images (repetition time, 610 ms; echo time, 22 ms) and T2-weighted spin-echo images (repetition time, 3,500 ms; echo time, 89 ms). Fat-suppressed images were also obtained. A slice thickness of 3 mm was chosen. The MRI diagnostic criteria for SONK included a discrete low-intensity area on the T1-weighted image and a corresponding low-intensity area with a surrounding high-intensity area, suggestive of bone marrow edema, on the T2-weighted and fat-suppressed images of the medial femoral condyle (Lotke and Ecker 1988, Lecouvet et al. 1998).

All the SONK patients had findings in the weight-bearing area on MRI. In addition, we used the necrotic angle to measure the size of the epiphyseal lesion on MRI (Mont et al. 2000). The arcs of involvement of the subchondral lesion were measured using the center of the radius of the lesion, as measured from the epiphyseal scar in the sagittal and coro-

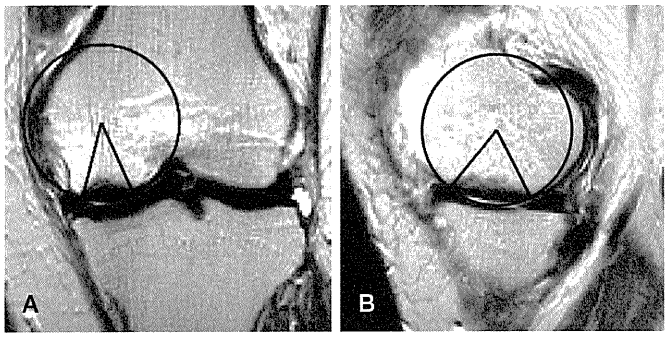

Figure 4. The necrotic angle (Mont et al. 2000) was measure in the sagittal plane (A) and the coronal plane (B). The 2 angles were summed to give the combined necrotic angle. In this case, the combined necrotic angle was 108° (40° + 68°).

nal planes (Figure 4). The 2 angles were summed to give the combined necrotic angle, which was used to assess the total lesions. Lesions of 150° or less were categorized as small, lesions of 151–249° were categorized as medium, and lesions of 250° or more were categorized as large.

BMD

We measured the BMD values at L2-L4 in the lumbar spine, the femoral neck, and the knee condyles using a QDR-4500 bone densitometer (Hologic Inc., Bedford, MA). We found no evidence of ipsilateral femoral neck BMD loss compared with the contralateral femoral neck BMD in either the SONK group or the OA group ($p = 0.9$ and $p = 0.4$, respectively). The BMD measurements for the knee condyles were performed with the patient in the supine position on the scanning table, with the knee flexed at an angle of 20° and the axis of the tibia parallel to the scanning table. In the tibial condyles, 5 square regions of interest were marked under a line on the proximal tibia. The medial tibial condyle BMDs in 2 medial square regions of interest and the lateral tibial condyle BMDs in 2 lateral square regions of interest were calculated for the tibia (Figure 5). In addition, we calculated the lateral and medial femoral condyle BMDs in square regions of interest of the same size as those on the proximal tibia marked on the femoral condyles. The ratios of the medial condyle BMD to the lateral condyle BMD (medial-lateral ratios) in the femur and tibia were used as parameters for comparisons of the BMDs at both condyles. Previous data have shown that this method is reliable (Akamatsu et al. 1997).

The patients were categorized according to the WHO definition (1994). A T-score of more than −1 was defined as normal, osteopenia was defined as a T-score of −1 to −2.49, and osteoporosis was defined as a T-score of −2.5 or less. In addition, low BMD was defined as a T score of −1 or less, which meant the sum of osteopenia and osteoporosis.

Statistics

Data were expressed as the mean with 95% confidence interval (CI). Values were checked for normal distribution with the Shapiro-Wilk test. Differences between the groups were determined by Student's t-test for continuous variables with normal distribution (age, height, weight, femorotibial angle, lumbar spine BMD, femoral neck BMD, lateral femoral condyle BMD, medial tibial condyle BMD, lateral tibial condyle BMD, and medial-lateral ratios); the Mann-Whitney test was used for continuous variables without normal distribution (BMI, Knee Society scores, and medial femoral condyle BMD); and the Pearson chi-square test (low BMD or normal based on the T scores at the lumbar spine) or Fisher's exact probability test (low BMD or normal based on the T-scores at the femoral neck) was used for nominal variables. SPSS software version 17 was used for the statistical analyses. Values of $p < 0.05$ were considered significant. We performed a priori power analysis to ensure that the study was not underpowered. Since were no similar previous studies, we compared the BMDs between the two groups using a Cohen's large effect size of 0.8 and a significance level of 0.05. We found that 80% power corresponded to a sample size of 26 subjects per group.

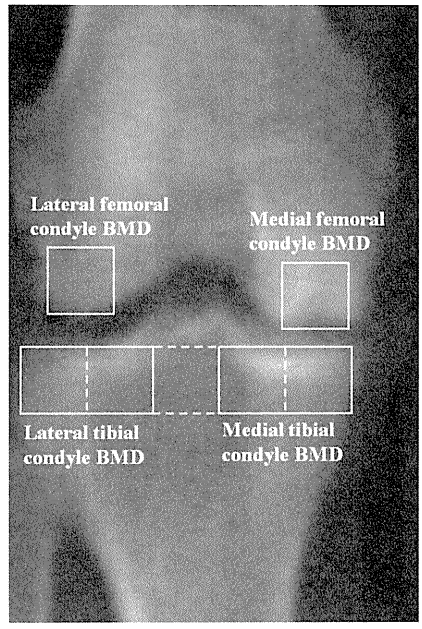

Figure 5. An AP dual X-ray absorptiometry image of the right knee of a 74-year-old woman 7 weeks after the onset of pain (the same patient as in Figure 2) showing a necrotic lesion surrounded by a sclerotic area in the medial femoral condyle. In the tibial condyles, five square regions of interest were marked on the frontal view. A line extending to the lateral and medial edges of the proximal tibia was divided into 5 equal lengths and 5 square regions of interest were marked underneath it. The medial tibial condyle BMDs in the 2 medial square regions of interest and the lateral tibial condyle BMDs in the 2 lateral square regions of interest were calculated for the tibia. In addition, the lateral and medial femoral condyle BMDs were calculated in square regions of interest of the same size as those on the tibial condyles located on a line passing through the tips of the medial and lateral condyles, with the midpoints of their distal sides at the points of contact.

Table 1. Patient characteristics. The values are given as mean (95% CI)

Variable	SONK (n = 26)	OA (n = 26)	95% CI for difference	p-value
Age, years	72 (70–74)	71 (68–73)	–1.5 to 4.7	0.3 [a]
Height, cm	150 (147–152)	152 (149–154)	–5.2 to 1.5	0.3 [a]
Weight, kg	55 (52–59)	55 (52–58)	–4.0 to 4.5	0.9 [a]
Body mass index, kg/m^2	25 (23–26)	24 (23–25)		0.4 [b]
Knee Society score, points				
Knee	53 (48–58)	72 (66–78)		< 0.001 [b]
Pain	20 (17–24)	35 (31–39)		< 0.001 [b]
Function	47 (40–53)	77 (68–86)		< 0.001 [b]

[a] Student's t-test.
[b] Mann-Whitney test.

Table 2. Imaging findings

Variable	SONK (n = 26)	OA (n = 26)	95% CI for difference	p-value
Femorotibial angle (°)	180 (179–181)	179 (178–190)	–0.2 to 2.1	0.1 [a]
Kellgren-Lawrence grade (knees)				
Grade 1	5	0		
Grade 2	19	8		
Grade 3–4	2	18		
Radiographic stage (knees)				
Stage 1	7			
Stage 2	19			
Stage 3 to 4	0			
Combined necrotic angle (°)	165 (154–176)			
Lesion size (knees)				
Small	7			
Medium	19			
Large	0			

[a] Student's t-test.

Results

2 of the authors (YA, NM) measured the femorotibial angle on 135 knee radiographs and the interobserver interclass correlation coefficient was 0.996. In addition, the same authors classified the SONK lesions, and the kappa coefficient to determine the interobserver agreement of the radiographic staging was 0.88.

At entry into the study, the mean Knee Society knee, pain, and function scores were higher in the OA group than in the SONK group (Table 1).

All knees with spontaneous osteonecrosis had femorotibial angles of more than 174°; the Kellgren and Lawrence grades were grade 1 in 5 knees, grade 2 in 19 knees, and grade 3 in 2 knees. In the OA group, the Kellgren and Lawrence grades were grade 2 in 8 knees and grades 3–4 in 18 knees. The radiographic stages of SONK at the time of diagnosis were stage 1 in 7 knees and stage 2 in 19 knees. The mean combined necrotic angle of the SONK group was 165°. Small lesions were noted in 7 knees and medium lesions were noted in 19 knees (Table 2).

The mean femoral neck BMD was lower in the SONK group than in the OA group (CI for difference: –0.12 to –0.04; $p < 0.001$). All the knees in the SONK group had low BMDs at the femoral neck, and 20 of 26 knees in the OA group had low BMDs at the femoral neck ($p = 0.02$). However, there was no statistically significant difference in mean lumbar spine BMD between the 2 groups. The mean lateral femoral and tibial condyle BMDs were significantly lower in the SONK group than in the OA group (CI for difference: –0.19 to –0.07, $p < 0.001$; and CI for difference: –0.20 to –0.06, $p < 0.001$, respectively). However, the mean medial femoral and medial tibial condyle BMDs were similar between the two groups. The mean femoral and tibial medial-lateral ratios were significantly higher in the SONK group than in the OA group (CI for difference: 0.17–0.58, $p = 0.001$; and CI for difference: 0.01–0.34, $p = 0.04$, respectively) (Table3).

Discussion

We found that BMD of the femoral neck, lateral femoral condyle, and lateral tibial condyle were significantly lower in the SONK patients than in the OA patients. Also, the femoral and tibial medial-lateral ratios were significantly higher in the SONK patients than in the OA patients. Our findings support the subchondral insufficiency fracture theory for the onset of SONK from low BMD in women > 60 years of age.

The SONK group had a significantly lower BMD at the femoral neck than the OA group, and all the SONK patients had low BMDs at the femoral neck. In addition, similar to the case of the femoral neck, the SONK group had significantly lower BMDs at the lateral femoral and lateral tibial condyles than the OA group. The lateral condyle BMDs represent the BMD of the ipsilateral lower extremity in all of the knee condyles, as we found in a previous study (Akamatsu et al. 2009). These findings therefore suggest that recent onset of SONK has an association with low BMD in women over 60 years. The SONK group had lower BMD values at the femoral neck, but not at the lumbar spine, than the OA group. The hip is less affected by OA with age than the spine. Because lumbar spine osteophytes affect most subjects over 60 years and indicate false higher lumbar spine BMD values, diagnosis of osteoporosis in the elderly should be based on hip BMD (Liu et al. 1997). We therefore evaluated the BMD values at the femoral neck.

Table 3. BMD at various locations and medial-lateral ratios. The values are given as mean (95% CI)

Variable	SONK (n = 26)	OA (n = 26)	95% CI for difference	p-value
Lumbar spine BMD, g/cm^2	0.79 (0.73–0.84)	0.84 (0.79–0.89)	–0.13 to 0.02	0.2 [b]
Based on the T score at the lumbar spine				
Low BMD [a] / Normal BMD (knees)	20 / 6	20 / 6		1.0
Femoral neck BMD, g/cm^2	0.54 (0.51–0.56)	0.62 (0.59–0.65)	–0.12 to –0.04	< 0.001 [b]
Based on the T score at the femoral neck				
Low BMD [a] / Normal BMD (knees)	26 / 0	20 / 6		0.01
Medial femoral condyle BMD, g/cm^2	1.04 (0.96–1.12)	1.02 (0.95–1.09)		1.0 [c]
Lateral femoral condyle BMD, g/cm^2	0.57 (0.53–0.61)	0.70 (0.65–0.75)	–0.19 to –0.07	< 0.001 [b]
Femoral medial-lateral ratio	1.86 (1.69–2.03)	1.48 (1.36–1.60)	0.17 to 0.58	0.001 [b]
Medial tibial condyle BMD, g/cm^2	0.78 (0.69–0.86)	0.82 (0.75–0.89)	–0.15 to 0.04	0.2 [b]
Lateral tibial condyle BMD, g/cm^2	0.52 (0.48–0.57)	0.65 (0.60–0.71)	–0.20 to –0.06	< 0.001 [b]
Tibial medial-lateral ratio	1.45 (1.31–1.59)	1.27 (1.18–1.36)	0.01 to 0.34	0.04 [b]

[a] Low BMD was defined as a T score of –1 or less.
[b] Student's t-test.
[c] Mann-Whitney test.

Abnormal medial-lateral ratio, which is a parameter for comparison of the medial condyle BMD with the lateral condyle BMD, in patients with knee OA is associated with increases in varus deformity (Akamatsu et al. 1997), bone marrow lesions, osteophytes, joint space narrowing, and sclerosis (Lo et al. 2006). We have found study on the comparison in the medial-lateral ratios between the SONK and the OA groups. The higher femoral medial-lateral ratio in the SONK group than in the OA group in our study corresponds to previous scintigraphic findings that the mean medial-lateral ratios of the distal femur plus proximal tibia in the early phase of SONK were higher than the ratios in knee OA (Muheim et al. 1970). We speculate these results show new bone formation accompanying the onset of SONK. We detected bone formation in the medial femoral condyle prior to the radiographic detection of the surrounding sclerotic halo.

Previous papers (Houpt et al. 1983, Mears et al. 2009, Robertson et al. 2009) have suggested the presence of preexisting knee OA in patients with SONK. It is likely that knee OA is common in women older than 60 years, and that most of our SONK patients had knee OA before the onset of osteonecrosis. We found Kellgren-Lawrence grades of 2 or higher in the knees of 21 of the 26 patients with SONK. This finding of preexisting knee OA in our SONK group is similar to published results (Houpt et al. 1983, Mears et al. 2009). Furthermore, overlying degenerative cartilage changes and medial meniscus or meniscal root injury (Ahlbäck et al. 1968, Robertson et al. 2009), which could be degenerative osteoarthritic changes, may weaken the load-bearing capacity (Narváez et al. 2003) and occur with increased loading at the medial femoral condyle, resulting in subchondral fracture. Thus, the pathogenesis of SONK may not only be related to low BMD but also to preexisting knee OA.

The degree of the combined necrotic angle on MRI correlates with the prognosis (Mont et al. 2000, Yates et al. 2007), with one report describing patients who had small combined necrotic angles of 150° or less and who were all clinically recovered at mean 5 months after the onset of disease (Yates et al. 2007). The mean combined necrotic angle in our SONK group was 165°. One reason for this difference may be related to the fact that our SONK patients all had lesions in the weight-bearing area, unlike in the previous study (Yates et al. 2007).

Our study design had several limitations. First, since we limited our study to subjects who presented within 3 months of the onset of clinical symptoms, only a small number of eligible patients were enrolled—and all cases were diagnosed with stage-1 or stage-2 disease using plain radiographs. The unremarkable radiographic changes delayed the diagnosis (Ahlbäck et al. 1968), and it was difficult to compile patients with SONK at the early stage after disease onset. Second, the lower Knee Society function score in the SONK group than in the OA group resulted from restricted activities of walking and climbing or descending stairs because of severe pain. However, we considered that limiting the duration to within 3 months of the onset of symptoms minimized the influence of disuse osteoporosis, because we found no evidence of differences between the bilateral femoral neck BMDs in the SONK group and the OA group at entry into our study. The distinctions between SONK and the osteonecrotic-like lesions found in knee OA using MRI were equivocal (Ahuja and Bullough 1978). Therefore, the criteria of typical clinical presentations (Ahlbäck et al. 1968, Lotke and Ecker 1988) and lesions in the weight-bearing area (Lotke and Ecker 1988) were essential for diagnosis of SONK in our study.

A recent report has indicated that the use of bisphosphonate prevents collapse in osteonecrosis of the femoral head (Lai et al. 2005). Future investigations should consider whether increasing the BMD, including the use of medications for osteoporosis, is an appropriate nonoperative approach to treatment of patients with SONK.

YA: study design, collection and interpretation of data, and statistical analysis. NM: study design and statistical analysis. TH and HK: collection of data. TS: study design and interpretation of data. All authors contributed to writing of the manuscript.

No competing interests declared.

Ahlbäck S. Osteoarthrosis of the knee: a radiographic investigation. Acta Radiol Diagn (Stockh) (Suppl 277) 1968: 7-72.

Ahlbäck S, Bauer G C, Bohne W H. Spontaneous osteonecrosis of the knee. Arthritis Rheum 1968; 11 (6): 705-33.

Ahuja S C, Bullough P G. Osteonecrosis of the knee: a clinicopathological study in twenty-eight patients. J Bone Joint Surg (Am) 1978; 60 (2): 191-7.

Akamatsu Y, Koshino T, Saito T, Wada J. Changes in osteosclerosis of the osteoarthritic knee after high tibial osteotomy. Clin Orthop 1997; (334): 207-14.

Akamatsu Y, Mitsugi N, Taki N, Takeuchi R, Saito T. Relationship between low bone mineral density and varus deformity in postmenopausal women with knee osteoarthritis. J Rheum 2009; 36 (3): 592-7.

Houpt J B, Pritzker K P, Alpert B, Greyson N D, Gross A E. Natural history of spontaneous osteonecrosis of the knee (SONK): a review. Semin Arthritis Rheum 1983; 13 (2): 212-27.

Hunter D J, Niu J, Felson D T, Harvey W F, Gross K D, McCree P, Aliabadi P, Sack B, Zhang Y. Knee alignment does not predict incident osteoarthritis: the Framingham Osteoarthritis Study. Arthritis Rheum 2007; 56 (4): 1212-8.

Insall J N, Dorr L D, Scott R D, Scott W N. Rationale of the Knee Society clinical rating system. Clin Orthop 1989; (248): 13-4.

Kellgren J H, Lawrence J S. Radiological assessment of osteo-arthrosis. Ann Rheum Dis 1957; 16 (4): 494-502.

Koshino T. The treatment of spontaneous osteonecrosis of the knee by high tibial osteotomy with and without bone-grafting or drilling of the lesion. J Bone Joint Surg (Am) 1982; 64 (1): 47-58.

Lai K A, Shen W J, Yang C Y, Shao C J, Hsu J T, Lin R M. The use of alendonate to prevent early collapse of the femoral head in patients with nontraumatic osteonecrosis. J Bone Joint Surg (Am) 2005; 87 (10): 2155-9.

Lecouvet F E, van de Berg B C, Maldague B E, Lebon C J, Jamart J, Saleh M, Noël H, Malghem J. Early irreversible osteonecrosis versus transient lesions of the femoral condyles: prognostic value of subchondral bone and marrow changes on MR imaging. Am J Roentgenol 1998; 170 (1): 71-7.

Liu G, Peacock M, Eilam O, Dorulla G, Braunstein E, Johnston C C. Effect of osteoarthritis in the lumbar spine and hip on bone mineral density and diagnosis of osteoporosis in elderly men and women. Osteoporos Int 1997; 7 (6): 564-9.

Lo G H, Zhang Y, McLennan C, Niu J, Kiel D P, McLean R R, Aliabadi P, Felson D T, Hunter D J. The ratio of medial to lateral tibial plateau bone mineral density and compartment-specific tibiofemoral osteoarthritis. Osteoarthritis Cartilage 2006; 14 (10): 984-90.

Lotke P A, Ecker M L. Osteonecrosis of the knee. J Bone Joint Surg (Am) 1988; 70 (3): 470-3.

Lotke P A, Ecker M L, Alavi A. Painful knees in older patients: radionuclide diagnosis of possible osteonecrosis with spontaneous resolution. J Bone Joint Surg (Am) 1977; 59 (5): 617-21.

Mears S C, McCarthy E F, Jones L C, Hungerford D S, Mont M A. Characterization and pathological characteristics of spontaneous osteonecrosis of the knee. Iowa Orthop J 2009; 29: 38-42.

Mont M A, Baumgarten K M, Rifai A, Bluemke D A, Jones L C, Hungerford D S. Atraumatic osteonecrosis of the knee. J Bone Joint Surg (Am) 2000; 82 (9): 1279-90.

Muheim G, Bohne W H. Prognosis in spontaneous osteonecrosis of the knee: investigation by radionuclide scintimetry and radiography. J Bone Joint Surg (Br) 1970; 52 (4): 605-12.

Narváez J A, Narváez J, De Lama E, Sánchez A. Spontaneous osteonecrosis of the knee associated with tibial plateau and femoral condyle insufficiency stress fracture. Eur Radiol 2003; 13 (8): 1843-8.

Robertson D D, Armfield D R, Towers J D, Irrgang J J, Maloney W J, Harner C D. Meniscal root injury and spontaneous osteonecrosis of the knee: an observation. J Bone Joint Surg (Br) 2009; 91 (2): 190-5.

Takeda M, Higuchi H, Kimura M, Kobayashi Y, Terauchi M, Takagishi K. Spontaneous osteonecrosis of the knee: histopathological differences between early and progressive cases. J Bone Joint Surg (Br) 2008; 90 (3): 324-9.

Yamamoto T, Bullough P G. Spontaneous osteonecrosis of the knee: the result of subchondral insufficiency fracture. J Bone Joint Surg (Am) 2000; 82 (6): 858-66.

Yates P J, Calder J D, Stranks G J, Conn K S, Peppercorn D, Thomas N P. Early MRI diagnosis and non-surgical management of spontaneous osteonecrosis of the knee. Knee 2007; 14 (2): 112-6.

Zanetti M, Romero J, Dambacher M A, Hodler J. Osteonecrosis diagnosed on MR images of the knee: relationship to reduced bone mineral density determined by high resolution peripheral quantitative CT. Acta Radiol 2003; 44 (5): 525-31.

Low-Intensity Pulsed Ultrasound Accelerates Fracture Healing by Stimulation of Recruitment of Both Local and Circulating Osteogenic Progenitors

Ken Kumagai,[1] Ryohei Takeuchi,[1] Hiroyuki Ishikawa,[1] Yuichiro Yamaguchi,[1] Takahiro Fujisawa,[1] Takashi Kuniya,[1] Shu Takagawa,[1] George F. Muschler,[2] Tomoyuki Saito[1]

[1]Department of Orthopaedic Surgery, Yokohama City University, Yokohama, Japan, [2]Department of Biomedical Engineering, Orthopaedic Research Center, Cleveland Clinic, Cleveland, Ohio

Received 25 May 2011; accepted 16 February 2012
Published online 14 March 2012 in Wiley Online Library (wileyonlinelibrary.com). DOI 10.1002/jor.22103

ABSTRACT: We investigated the effect of low-intensity pulsed ultrasound (LIPUS) on the homing of circulating osteogenic progenitors to the fracture site. Parabiotic animals were formed by surgically conjoining a green fluorescent protein (GFP) mouse and a syngeneic wild-type mouse. A transverse femoral fracture was made in the contralateral hind limb of the wild-type partner. The fracture site was exposed to daily LIPUS in the treatment group. Animals without LIPUS treatment served as the control group. Radiological assessment showed that the hard callus area was significantly greater in the LIPUS group than in the control group at 2 and 4 weeks post-fracture. Histomorphometric analysis at the fracture site showed a significant increase of GFP cells in the LIPUS group after 2 weeks (7.5%), compared to the control group (2.4%) ($p < 0.05$). The LIPUS group exhibited a significantly higher percentage of GFP cells expressing alkaline phosphatase (GFP/AP) than the control group at 2 weeks post-fracture (5.9%, 0.3%, respectively, $p < 0.05$). There was no significant difference in the percentage of GFP/AP cells between the LIPUS group (2.0%) and the control group (1.4%) at 4 weeks post-fracture. Stromal cell derived factor-1 and CXCR4 were immunohistochemically identified at the fracture site in the LIPUS group. These data indicate that LIPUS induced the homing of circulating osteogenic progenitors to the fracture site for possible contribution to new bone formation. © 2012 Orthopaedic Research Society. Published by Wiley Periodicals, Inc. J Orthop Res 30:1516–1521, 2012

Keywords: LIPUS; fracture healing; circulating osteogenic progenitors; homing

Successful fracture healing requires the proliferation and migration of osteogenic cells into the fracture callus.[1] To promote fracture healing, a variety of treatment techniques have been developed. Low-intensity pulsed ultrasound (LIPUS) therapy is well recognized as one beneficial procedure enabling fractures to be treated without surgical invasion. LIPUS stimulation is said to increase the rate of osteogenic differentiation of stem and progenitor cells.[2,3]

LIPUS is a source of mechanical energy transmitted as high-frequency acoustical pressure waves into biological tissues.[4] It has been generalized that the micromechanical strains generated by these pressure waves evoke biochemical events that can regulate fracture healing.[5] Despite clinical and experimental studies demonstrating the enhancing effects of LIPUS on bone regeneration,[4–7] the biophysical mechanisms involved in the fracture healing process remain unclear, and require further study.

The biology of fracture healing is a complex physiological process including: formation of early fracture hematoma; an initial inflammatory response characterized by chemotaxis and migration of inflammatory cells; proliferation and differentiation of local osteogenic progenitors; revascularization and remodeling. All of these processes are regulated by local factors, cytokines or systemic hormones, involved in intramembranous and endochondral ossification.[8,9] LIPUS may act on the cellular reactions in each stage of the fracture healing process.[6] However, bone formation requires a source of osteoblasts.[10–12] Recent investigations have shown osteogenic connective tissue progenitor cells to be present in the systemic circulation and to contribute to fracture healing.[13,14] Recruitment of progenitor cells through the systemic circulation may have therapeutic potential for fracture healing.

This study was designed to test the hypothesis that LIPUS stimulates the homing of circulating osteogenic progenitors to the fracture site and enhances fracture healing.

METHODS

Animal Model

Twenty pairs of transgenic green fluorescent protein (GFP+) mice (C57BL/6-Tg CAG-EGFP) and wild-type C57BL/6 mice were purchased from the Japan SLC, Inc. (Hamamatsu, Japan). All animal protocols were approved by our Institutional Animal Care and Use Committees. A parabiotic mouse model was created at 12 weeks of age, as previously described.[14] One transgenic GFP mouse and one wild-type mouse were surgically conjoined from the olecranon to the knee joint on corresponding lateral aspects under general anesthesia with isoflurane.

Creation of Fracture

Three weeks after parabiosis surgery, a transverse femoral fracture was created in the wild-type partner. After anesthetizing the parabiotic animals with isoflurane, the contralateral hind limb of the wild-type partner was shaved and disinfected. A lateral incision was made along the midshaft of the femur. The muscles were separated bluntly, exposing the femur. The diaphysial femur was osteotomized transversely using a circular saw. To create a "challenged" fracture, 2 mm of periosteum was stripped circumferentially

Correspondence to: Ken Kumagai (T: 81-45-787-2655; F: 81-45-781-7922; E-mail: kumagai@yokohama-cu.ac.jp)

at both edges of the osteotomy site. The fracture was stabilized with an intramedullary pin.

LIPUS Intervention

The fracture site was treated with daily LIPUS exposure for 20 min using a clinical device (Sonic Accelerated Fracture Healing System, Smith & Nephew Inc., Memphis, TN). The LIPUS signal was composed of a 1.5 MHz ultrasound wave delivered at a frequency of 1 kHz in 200 μs pulses, and provided an average 30 mW/cm^2 spatial and temporal intensity. A transducer was placed on the medial aspect of the shaved thigh with ultrasound gel under general anesthesia in the both groups. The LIPUS signal was generated through the transducer in the treatment group. No ultrasound intervention was applied to the control group. The LIPUS treatment was continued daily until the termination of the experiment (2 or 4 weeks after fracture). Five parabiotic pairs were used at each time point in each treatment group.

Radiological Assessment

The animals were euthanized with a carbon dioxide inhalation at two or four weeks after fracture. Ventro-dorsal X-rays of the healed femora were taken using a Softex CSM soft X-ray system (Softex Co., Ltd, Tokyo, Japan). Radiographs of each femur were digitally captured with a scanner. The external hard callus area was measured as previously described.[6] The region of interest for the external hard callus was traced, and the number of pixels was measured using Image-Pro Plus software (Media Cybernetics, Silver Spring, MD). This pixel value was converted to mm^2.

Histological Assessment

The femora were carefully dissected and the intramedullary pins were removed. Each tissue sample was fixed in 4% paraformaldehyde at 4°C for 24 h, decalcified in an EDTA-based decalcifying solution (Osteosoft; Merck, Darmstadt, Germany) at 4°C for 5 days and cryoprotected by overnight incubation in 15% sucrose at 4°C. For cryosection, specimens were quickly frozen in an optimum cutting temperature (OCT) compound (Tissue-Tek OCT compound; Sakura Finetek Co. Ltd, Tokyo, Japan). OCT-embedded tissues were stored in the dark at −80°C. The center of the fracture region was longitudinally cryosectioned at 5 μm thickness from OCT-embedded tissue using a Leica CM3050 cryotome (Leica Microsystems, Heidelberg, Germany). To confirm osteogenic differentiation, staining to detect alkaline phosphatase (AP) activity[15] was performed using a Vector Red alkaline phosphatase Substrate Kit I (SK-5100; Vector Laboratories, Burlingame, CA) according to the manufacturer's instructions. The slides were mounted with aqueous mounting medium containing 4′-6′-diaminido-2-phenylindole (DAPI) (Vectashield Mounting Medium with DAPI H-1200; Vector Laboratories) to stain DNA. Additional sections of the fracture callus were stained with hematoxylin and eosin.

Immunohistochemistry

After washing with phosphate-buffered saline (PBS), the sections were blocked with normal goat serum for 30 min. Slides were then incubated for 120 min with either rabbit polyclonal anti-SDF-1 antibody diluted 1:200 (eBioscience, Inc., San Diego, CA) or rabbit polyclonal anti-CXCR4 antibody diluted 1:200 (Novus Biologicals Inc., Littleton, CO). Subsequently, all sections were washed with PBS and incubated for 60 min with Alexa Fluor 568 goat anti-rabbit IgG secondary antibody (Molecular Probes, Eugene, OR). Then, the sections were mounted with aqueous mounting medium containing DAPI (Vectashield Mounting Medium with DAPI H-1200; Vector Laboratories).

Histomorphometrical Quantification

The sections of the fracture site were analyzed by laser scanning confocal microscopy, using a Leica DM IRBE (TCS–SP–AOBS) Confocal Laser Scanning Microscope (Leica Microsystems). For confocal microscopy, three lasers were used: with a 351 nm UV excitation line for DAPI; a 488 nm Ar excitation line for GFP; and a 568 nm Kr excitation line for AP and Alexa Fluor 568. Emissions from DAPI, GFP, and AP were detected with a spectrophotometer at 400–460 nm, 500–550 nm, and 575–670 nm, respectively. Digital images from three high-power fields (375 μm^2) per section were acquired for cell counting. To limit potential bias in field selection, each field was chosen by DAPI staining and then scanned to obtain DAPI, GFP, and AP images. These images were processed using Image-Pro Plus software. Numbers of cells were determined by counting cell nuclei in the DAPI-stained images. Subsequently, DAPI images were co-localized with the GFP and AP images. All image processing was automated using custom-written programs for the batch processing of images.

Statistical Analysis

Analysis of variance (ANOVA) was used to test for significant differences among the test groups. The analysis was done using SigmaStat 3.5 software (Systat Software, Inc., Richmond, CA). In those instances where a significant difference was detected, Tukey–Kramer post hoc pairwise test of the means as well as post hoc test of the means against the control was performed. An adjusted p-value < 0.05 was considered statistically significant.

RESULTS

Post-Operative Status of Parabiotic Animals

Post-operatively, all animals recovered on the day of parabiosis surgery and rapidly learned to move together, cooperating in walking, and taking turns when getting access to food and water. Three parabiotic pairs died during the experimental period. One was dead before fracture surgery, one was dead from the LIPUS treatment group, and the other was dead from the control group. These animals were eliminated from analysis and were replaced.

Radiological Assessment

Callus formation could be detected at 2 weeks post-fracture, and bony bridging at the fracture site was confirmed at 4 weeks post-fracture (Fig. 1A). Radiographs at 4 weeks post-fracture in the LIPUS group exhibited newly formed bridging bone on both cortices at the fracture site in all cases. In contrast, radiographs of the control group at 4 weeks post-fracture showed bridging of the fracture gap in only 1 of 5 femora. The hard callus area in the LIPUS group was significantly greater than that in the control group at 2 weeks (3.7 ± 0.9 mm^2 vs. 0.4 ± 0.2 mm^2 respectively; $p < 0.05$) and 4 weeks (4.5 ± 2.1 mm^2 vs.

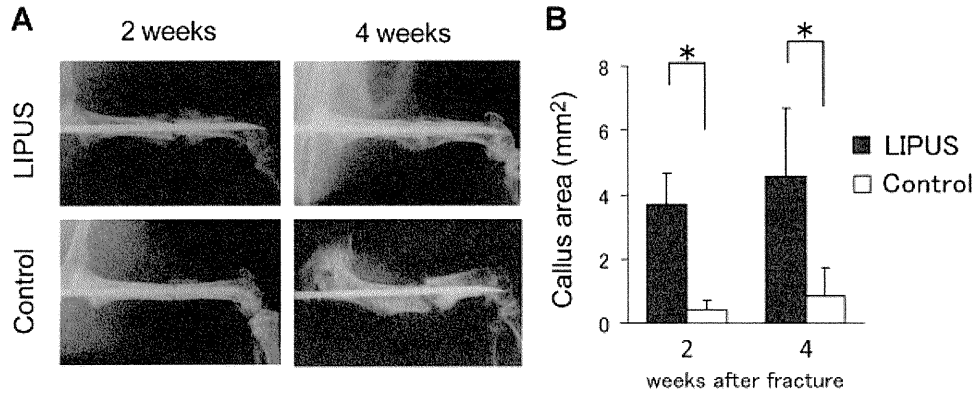

Figure 1. Radiological assessment of fracture healing. (A) Representative radiographs of LIPUS-treated femur and non-treated femur (control) at 2 and 4 weeks post-fracture. Bone union is completed in the LIPUS-treated femur at 4 weeks post-fracture. (B) Measurement of hard callus area in LIPUS group and control group. Values are given as mean ± SD ($n = 5$); difference from control $^{*}p < 0.05$.

0.9 ± 0.8 mm^2 respectively; $p < 0.05$) post-fracture (Fig. 1B).

Histological Assessment

Histological findings at the fracture site in the LIPUS group revealed bridging of the osteotomy site by external callus formation with woven bone (Fig. 2A). In contrast, no bone formation occurred around the osteotomy site in the control group (Fig. 2B). Positive AP expression was observed at the fracture callus in the LIPUS group (Fig. 2C), whereas less alkaline phosphatase expression was seen in the control group (Fig. 2D).

Homing of the Circulating Cells to the Fracture Region

GFP cells gaining access to the fracture site via the systemic circulation were identified in all animals in both groups at each time point ($n = 20/20$) (Fig. 3). The mean percentage of GFP cells in the LIPUS group (7.6%) was significantly higher than in the control group (2.4%) at 2 weeks post-fracture ($p < 0.05$) (Fig. 4A). In the control group, the percentage of GFP cells increased significantly between 2 and 4 weeks post-fracture. There was no significant difference in GFP cell ratios between the LIPUS group (7.4%) and the control group (6.3%) at 4 weeks post-fracture. In the total numbers of cells including both GFP positive cells and negative ones, the LIPUS group exhibited significantly greater AP expression than the control group at 2 weeks post-fracture (77.9% and 9.2%, respectively; $p < 0.05$). The mean percentage of AP expression decreased at 4 weeks in the LIPUS group (36.4%) whereas it increased in the control group (25.8%) (Fig. 4B). To evaluate the possible contribution of GFP cells to osteogenesis, co-localization of GFP and AP expression was assessed at both time points. The LIPUS group exhibited a significantly higher percentage of GFP cells with AP activity (GFP/AP) than the control group at 2 weeks post-fracture (5.9% and 0.3%, respectively; $p < 0.05$; Fig. 4C). There was no significant difference in the percentage of GFP/AP between

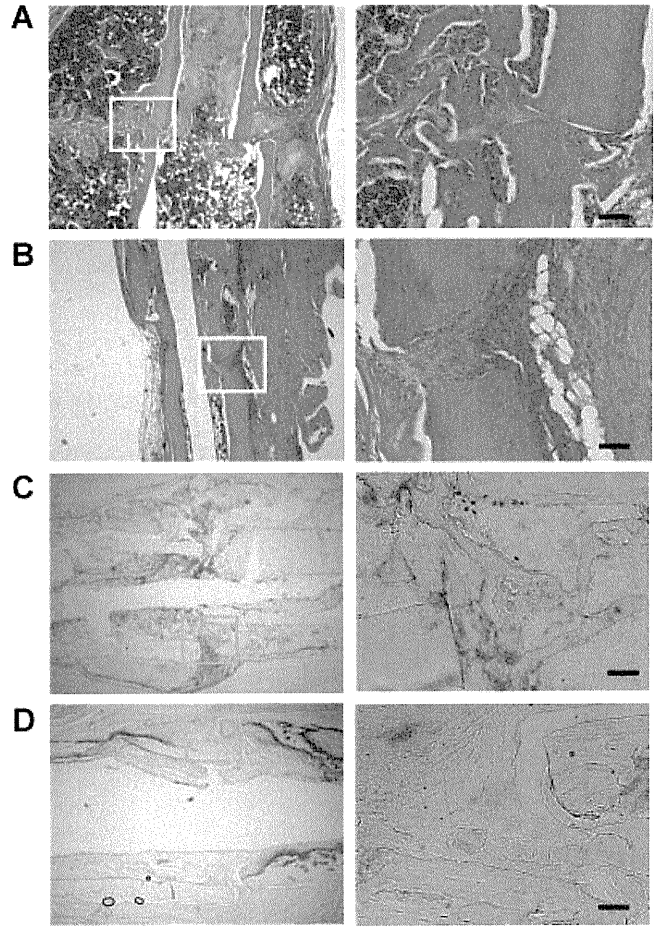

Figure 2. Histological findings at fracture site. (A and B) Representative photomicrographs of fracture site in LIPUS group (A) and control group (B) at 4 weeks post-fracture stained with hematoxylin and eosin. The LIPUS group shows new bone formation around the fracture gap. The control group shows the presence of fibrous tissue in the fracture gap. (C and D) Representative photomicrographs of fracture site stained for alkaline phosphatase (red) in LIPUS group (C) and control group (D) at 2 weeks post-fracture. Boxed areas in left-hand panels are shown at higher magnification at a single plane in right-hand panels. Scale bars indicate 50 μm.

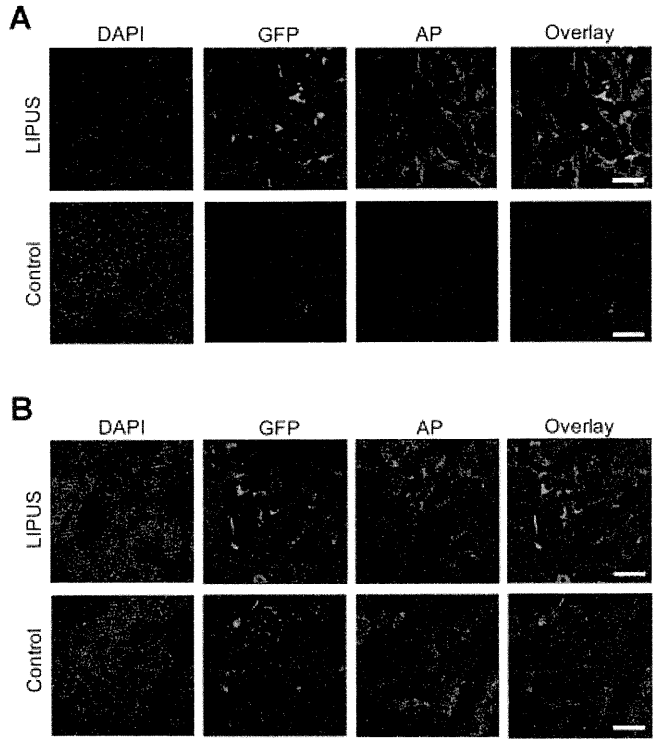

Figure 3. Confocal micrographs of fracture callus in parabiotic wild-type partners at 2 weeks (A) and 4 weeks (B) post-fracture. Each row represents DAPI (blue), GFP (green), alkaline phosphatase (AP, red), and Overlay (GFP/AP). (A) GFP positive cells are co-localized with regions of AP expression in LIPUS group. Less GFP and AP expressions are shown in control group. (B) Expression levels of GFP and AP are similar in both groups. Scale bars (right panels) indicate 50 μm.

the LIPUS group (2.0%) and the control group (1.4%) at 4 weeks post-fracture.

Immunohistochemistry

To assess the effect of LIPUS on the homing of circulating cells through the SDF-1/CXCR4 pathway, the expression of SDF-1 and CXCR4 was immunohistochemically examined. SDF-1 positive cells were identified at the fracture site in the LIPUS group (Fig. 5A). Expression of CXCR4 was clearly observed at the fracture site in the LIPUS group and was co-localized with GFP positive cells (Fig. 5B). In contrast, less expression of SDF-1 and CXCR4 was shown in the control group.

DISCUSSION

In general, most studies of fracture healing have focused on the contribution of local progenitors at the fracture site, or transplanted cells derived from cancellous bone or bone marrow. Recent focus has been directed at the possible contribution of circulating osteogenic progenitors that are recruited to the fracture site.[16,17] Several studies have suggested that osteogenic connective tissue progenitor cells may travel through the systemic circulation,[13,18] although the extent to which circulating osteogenic cells contribute

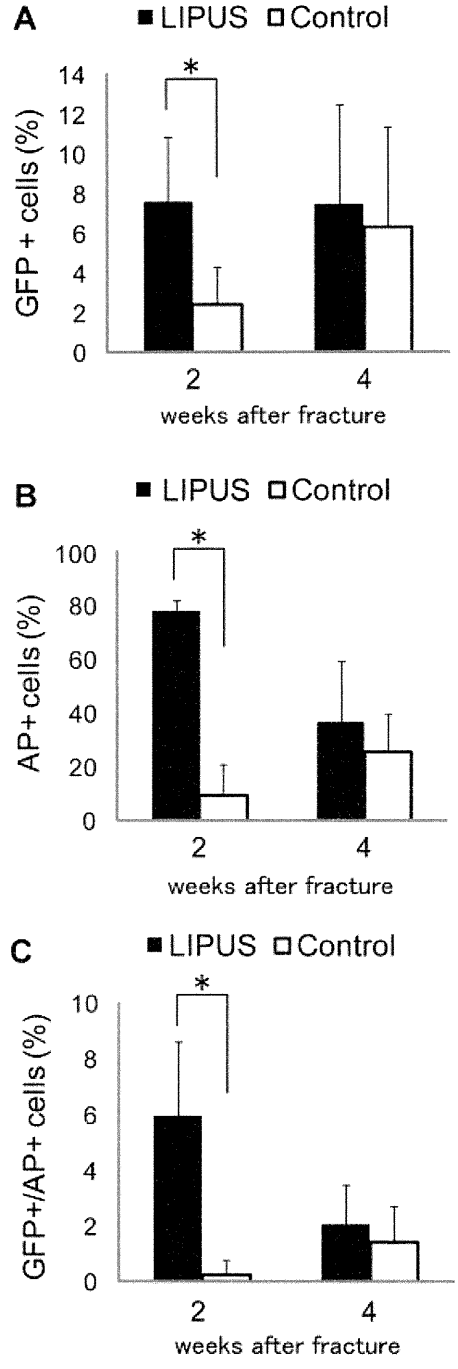

Figure 4. Histomorphometric quantification of cells expressing GFP and alkaline phosphatase (AP) in the fracture callus. The percentages of partner-derived GFP+ cells among all cells within the fracture callus are shown in (A). The percentages of all cells expressing AP are shown in (B). The percentages of the cells expressing both GFP and AP are shown in (C). Values are given as mean ± SD ($n = 5$); difference from control $^{*}p < 0.05$.

to normal fracture repair is only beginning to be characterized.[1] Previous work with a parabiotic mouse model has shown that circulating osteogenic cells home to the site of a fibular fracture and homing of osteogenic cells through the circulation increases during the period between 7 and 14 days post-fracture.[14] The data in this study also revealed LIPUS stimulates

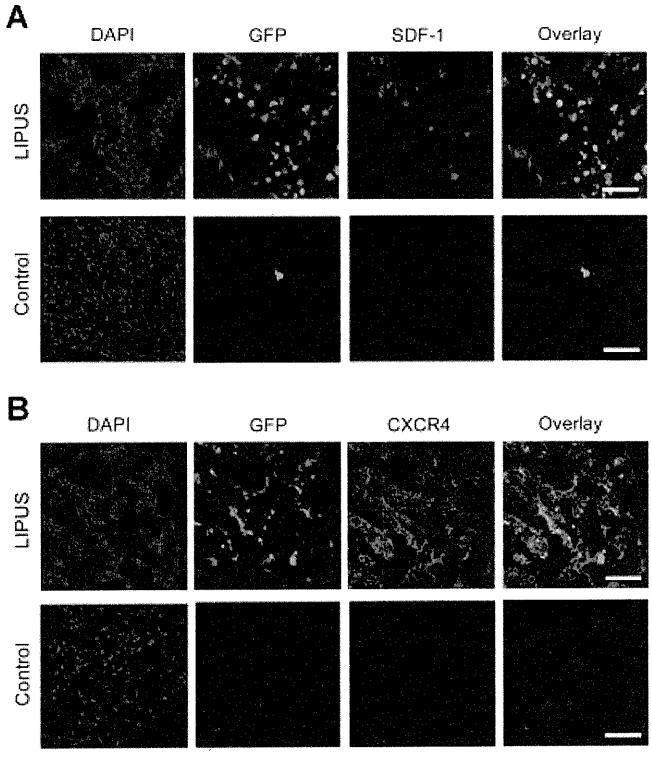

Figure 5. Confocal micrographs of fracture callus at 2 weeks. (A) Immunofluorescence staining of cell nuclei (DAPI, blue), GFP (green), and SDF-1 (Alexa Fluor 568, red). Scale bars (right panels) indicate 50 μm. (B) Immunofluorescence staining of cell nuclei (DAPI, blue), GFP (green), and CXCR4 (Alexa Fluor 568, red). Scale bars (right panels) indicate 50 μm.

the homing of circulating cells at 2 weeks post-fracture. These results seem to imply the effect of LIPUS on acceleration of fracture healing by recruitment of circulating osteogenic cells is limited up to the early stage of hard callus formation.

Nonunion is a common complication in the treatment of fractures, and numerous studies regarding fracture healing have referred to this problem. Reliable nonunion models have been achieved with rotational instability,[19] distraction force,[20] periosteal stripping,[21] periosteal cauterization on each side of the fracture,[22] segmental bony defect,[23] or a combination of periosteal stripping with segmental defect.[24] Recent investigations have reported that open osteotomy with intramedullary stabilization leads to pronounced delayed union compared with the standard rodent closed fracture model.[25,26] Takikawa et al.[7] showed that LIPUS promoted fracture healing in an experimental study using a rat nonunion model by muscle interposition in the fractured tibia. The model of an open osteotomy with a partial periosteal removal was used in this study to simulate the conditions where complete preservation of the periosteum is difficult. This setting occurs as a result of treatment for an open fracture or surgical technique in osteotomy. In case of partial loss of the periosteum, LIPUS may assist the initiation of the healing process since intramembraneous bone formation starts periosteally, some distance from the fracture gap.[5] The data in the present study suggest that LIPUS accelerates fracture healing by stimulating recruitment of osteogenic progenitors to the site of bone formation near the fracture site. However, this effect may be limited according to amount of the residual periosteum at the fracture site; that is, populations of local periosteal precursor may not have been completely replaced.

The maturation, trafficking and homing of stem and progenitor cells are known to be regulated by numerous chemokines and molecules.[27] SDF-1, a CXC chemokine, induces the recruitment of stem and progenitor cells to areas of tissue damage.[28] The interaction of SDF-1 and its receptor, CXCR4, plays a key role in the homing of circulating cells, and tissue preservation and repair.[29,30] A recent study reported that SDF-1 is induced in the periosteum of injured bone and promotes endochondral bone repair by recruiting mesenchymal stem cells to the site of injury.[31] Furthermore, migration of circulating mesenchymal stem cells in response to a bone fracture site has been reported to be dependent on the presence of CXCR4.[32]

In summary, this study demonstrated that bone formation was stimulated by LIPUS exposure at the site of a mouse femoral fracture with partial periosteal stripping. The data also suggested that LIPUS induced the homing of circulating osteogenic progenitors to the fracture site for possible contribution to new bone formation. In a setting where the local progenitor population is deficient, delivery of osteogenic progenitor cells and bone formation are limited through the fracture healing process.[1,12] The homing of osteogenic progenitors from the systemic circulation may complement local progenitors through intrinsic biological processes, although further study is necessary to confirm and extend these findings.

ACKNOWLEDGMENTS

This work was supported by Grant-in-Aid for Scientific Research from Ministry of Education, Culture, Sports, Science and Technology of Japan (#20591763).

REFERENCES

1. Patterson TE, Kumagai K, Griffith L, et al. 2008. Cellular strategies for enhancement of fracture repair. J Bone Joint Surg Am 90:111–119.
2. Ikeda K, Takayama T, Suzuki N, et al. 2006. Effects of low-intensity pulsed ultrasound on the differentiation of C2C12 cells. Life Sci 79:1936–1943.
3. Takayama T, Suzuki N, Ikeda K, et al. 2007. Low-intensity pulsed ultrasound stimulates osteogenic differentiation in ROS 17/2.8 cells. Life Sci 80:965–971.
4. Rubin C, Bolander M, Ryaby JP, et al. 2001. The use of low-intensity ultrasound to accelerate the healing of fractures. J Bone Joint Surg Am 83-A:259–270.
5. Claes L, Willie B. 2007. The enhancement of bone regeneration by ultrasound. Prog Biophys Mol Biol 93:384–398.
6. Azuma Y, Ito M, Harada Y, et al. 2001. Low-intensity pulsed ultrasound accelerates rat femoral fracture healing by acting on the various cellular reactions in the fracture callus. J Bone Miner Res 16:671–680.

7. Takikawa S, Matsui N, Kokubu T, et al. 2001. Low-intensity pulsed ultrasound initiates bone healing in rat nonunion fracture model. J Ultrasound Med 20:197–205.
8. Dimitriou R, Tsiridis E, Giannoudis PV. 2005. Current concepts of molecular aspects of bone healing. Injury 36: 1392–1404.
9. Einhorn TA. 1998. The cell and molecular biology of fracture healing. Clin Orthop Relat Res 355:S7–S21.
10. Muschler GF, Midura RJ. 2002. Connective tissue progenitors: practical concepts for clinical applications. Clin Orthop Relat Res 395:66–80.
11. Muschler GF, Midura RJ, Nakamoto C. 2003. Practical modeling concepts for connective tissue stem cell and progenitor compartment kinetics. J Biomed Biotechnol 2003: 170–193.
12. Muschler GF, Nakamoto C, Griffith LG. 2004. Engineering principles of clinical cell-based tissue engineering. J Bone Joint Surg Am 86-A:1541–1558.
13. Eghbali-Fatourechi GZ, Lamsam J, Fraser D, et al. 2005. Circulating osteoblast-lineage cells in humans. N Engl J Med 352:1959–1966.
14. Kumagai K, Vasanji A, Drazba JA, et al. 2008. Circulating cells with osteogenic potential are physiologically mobilized into the fracture healing site in the parabiotic mice model. J Orthop Res 26:165–175.
15. Miao D, Scutt A. 2002. Histochemical localization of alkaline phosphatase activity in decalcified bone and cartilage. J Histochem Cytochem 50:333–340.
16. Hou Z, Nguyen Q, Frenkel B, et al. 1999. Osteoblast-specific gene expression after transplantation of marrow cells: implications for skeletal gene therapy. Proc Natl Acad Sci USA 96:7294–7299.
17. Shirley D, Marsh D, Jordan G, et al. 2005. Systemic recruitment of osteoblastic cells in fracture healing. J Orthop Res 23:1013–1021.
18. Alm JJ, Koivu HM, Heino TJ, et al. 2010. Circulating plastic adherent mesenchymal stem cells in aged hip fracture patients. J Orthop Res 28:1634–1642.
19. Hietaniemi K, Peltonen J, Paavolainen P. 1995. An experimental model for non-union in rats. Injury 26:681–686.
20. Choi P, Ogilvie C, Thompson Z, et al. 2004. Cellular and molecular characterization of a murine non-union model. J Orthop Res 22:1100–1107.
21. Utvag SE, Grundnes O, Reikeraos O. 1996. Effects of periosteal stripping on healing of segmental fractures in rats. J Orthop Trauma 10:279–284.
22. Kokubu T, Hak DJ, Hazelwood SJ, et al. 2003. Development of an atrophic nonunion model and comparison to a closed healing fracture in rat femur. J Orthop Res 21:503–510.
23. Russell G, Tucci M, Conflitti J, et al. 2007. Characterization of a femoral segmental nonunion model in laboratory rats: report of a novel surgical technique. J Invest Surg 20: 249–255.
24. Garcia P, Holstein JH, Maier S, et al. 2008. Development of a reliable non-union model in mice. J Surg Res 147:84–91.
25. Kratzel C, Bergmann C, Duda G, et al. 2008. Characterization of a rat osteotomy model with impaired healing. BMC Musculoskelet Disord 9:135.
26. Oetgen ME, Merrell GA, Troiano NW, et al. 2008. Development of a femoral non-union model in the mouse. Injury 39:1119–1126.
27. Baggiolini M. 1998. Chemokines and leukocyte traffic. Nature 392:565–568.
28. Ceradini DJ, Kulkarni AR, Callaghan MJ, et al. 2004. Progenitor cell trafficking is regulated by hypoxic gradients through HIF-1 induction of SDF-1. Nat Med 10:858–864.
29. Otsuru S, Tamai K, Yamazaki T, et al. 2008. Circulating bone marrow-derived osteoblast progenitor cells are recruited to the bone-forming site by the CXCR4/stromal cell-derived factor-1 pathway. Stem Cells 26:223–234.
30. Penn MS. 2010. SDF-1:CXCR4 axis is fundamental for tissue preservation and repair. Am J Pathol 177:2166–2168.
31. Kitaori T, Ito H, Schwarz EM, et al. 2009. Stromal cell-derived factor 1/CXCR4 signaling is critical for the recruitment of mesenchymal stem cells to the fracture site during skeletal repair in a mouse model. Arthritis Rheum 60:813–823.
32. Granero-Molto F, Weis JA, Miga MI, et al. 2009. Regenerative effects of transplanted mesenchymal stem cells in fracture healing. Stem Cells 27:1887–1898.

Arthritis Care & Research
Vol. 64, No. 7, July 2012, pp 1036–1045
DOI 10.1002/acr.21651

ORIGINAL ARTICLE

Medial Versus Lateral Condyle Bone Mineral Density Ratios in a Cross-Sectional Study: A Potential Marker for Medial Knee Osteoarthritis Severity

YASUSHI AKAMATSU, NAOTO MITSUGI, NAOYA TAKI, HIDEO KOBAYASHI, AND TOMOYUKI SAITO

Objective. To assess the association of bone mineral density (BMD) of the femoral and tibial condyles with knee pain and disease severity in women with symptomatic medial knee osteoarthritis (OA).

Methods. We enrolled 192 women (ages 41–90 years) between April 2007 and March 2011. The subjects were divided into 2 groups according to joint space narrowing (JSN) on weight-bearing radiographs. BMD of the lumbar spine, proximal femur, and knee condyles was measured. Medial and lateral condyle BMDs of the femur and tibia as well as the medial versus lateral condyle BMD ratios were measured.

Results. Mean medial condyle BMDs, medial versus lateral condyle BMD ratios, and visual analog scale (VAS) pain in both the femur and the tibia were higher in the obliteration group compared with the narrowing group ($P < 0.001$ for all). A significant positive correlation was observed between the femoral and tibial condyles in the following parameters: medial condyle BMDs, lateral condyle BMDs, and medial versus lateral condyle BMD ratios ($r = 0.791–0.844$). In both the femur and the tibia, medial versus lateral condyle BMD ratios had significant positive correlations with femorotibial angle, medial osteophytes, lateral osteophytes, medial JSN, and VAS pain, and had significant negative correlations with the Knee Society pain and function scores.

Conclusion. Although this study was a cross-sectional study, the femoral and tibial medial versus lateral condyle BMD ratios increased with more severe knee pain and might be a potential marker for monitoring disease severity in women with symptomatic medial knee OA.

INTRODUCTION

Abnormal medial loading results in decreased cartilage thickness, osteophyte ingrowth, and subchondral bone sclerosis in the medial femoral and tibial condyles (1). Among these changes, subchondral bone sclerosis may reflect altered mechanical loading. Subchondral bone plays an important role in the incidence (2) and progression (3) of knee osteoarthritis (OA). Altman and Gold have presented an atlas of radiographic features to identify the presence or absence of subchondral bone sclerosis (4); however, sclerosis of the knee condyles remains difficult to visually discern on radiographs (5,6). Various noninvasive studies have attempted to quantify the alterations in bone anatomy in response to altered mechanical loading using scintigraphy (7), bone densitometry (8–10), fractal radiography (11), and magnetic resonance imaging (MRI) (12). Recently, bone mineral density (BMD) was measured using dual x-ray absorptiometry (DXA) in the tibial condyles of healthy subjects (13,14), random populations (15,16), subjects with radiographic knee OA (17–20), and subjects with symptomatic knee OA (5,21–24). The advantage of this measurement is that the BMD value increases in the subchondral bone of tibial condyles prior to radiographic progression (15). In the present study, we measured not only the tibial condyle BMD but also the femoral condyle BMD, unlike other studies (13,15–24), and have developed medial versus lateral condyle BMD ratios for the femur and tibia (25). Abnormal medial versus lateral condyle BMD ratios are associated with an increase of

Yasushi Akamatsu, MD, PhD, Naoto Mitsugi, MD, PhD, Naoya Taki, MD, Hideo Kobayashi, MD, PhD, Tomoyuki Saito, MD, PhD: Yokohama City University, Yokohama, Japan.

Address correspondence to Yasushi Akamatsu, MD, PhD, Department of Orthopaedic Surgery, Yokohama City University School of Medicine, 3-9 Fukuura, Kanazawa-ku, Yokohama 236-0004, Japan. E-mail: akamatsu@yokohama-cu.ac.jp.

Submitted for publication August 4, 2011; accepted in revised form February 20, 2012.

Significance & Innovations

- In women with symptomatic medial knee osteoarthritis (OA), mean medial condyle bone mineral densities (BMDs), medial versus lateral condyle BMD ratios, and visual analog scale (VAS) pain in both the femur and the tibia were significantly higher in patients with joint space obliteration compared with patients with joint space narrowing (JSN).
- After adjusting for age and body mass index, femoral and tibial medial versus lateral condyle BMD ratios demonstrated significant positive correlations with knee alignment, presence of medial and lateral osteophytes, medial JSN, and VAS pain, whereas they demonstrated significant negative correlations with knee pain and function scores.
- The results of this cross-sectional study indicated that the femoral and tibial medial versus lateral condyle BMD ratios increased with more severe knee pain and might be a potential marker for monitoring disease severity in women with symptomatic medial knee OA.

varus deformity (25), peak knee adduction moment (21), bone marrow lesions (17), osteophytes, joint space narrowing (JSN), sclerosis (18), and meniscal damage (19).

To the best of our knowledge, the medial and lateral condyle BMDs and medial versus lateral condyle BMD ratios in both the femur and the tibia have only been measured in a previous study that we performed (25). In addition, knee pain is associated with joint effusion, synovitis, cartilage volume, bone marrow edema, and denuded bone (26–30). However, no studies comparing subchondral bone sclerosis in the knee condyles with knee pain have previously been reported. This cross-sectional DXA study selected patients with symptomatic medial knee OA and investigated the severity of OA in progressive stages in relation to BMD in the condyles, which might possibly be a biomarker for monitoring the severity of medial knee OA. The aim of our present study was to assess the association between BMD of the femoral and tibial condyles and knee pain in women with symptomatic medial knee OA. We investigated the differences in BMD of the femoral and tibial condyles and knee pain with cases between JSN and joint space obliteration as observed on radiographs, and the relationship of medial and lateral condyle BMDs and medial versus lateral condyle BMD ratios between the femoral and tibial condyles, as well as their correlation with knee pain and other factors.

PATIENTS AND METHODS

Participants. We conducted a cross-sectional study between April 2007 and March 2011 on a convenience sample at our institution. A total of 348 consecutive patients were initially screened. All patients had symptomatic primary knee OA and had experienced chronic knee pain for >3 months, and reported knee pain during walking and ascending and/or descending stairs. No patient reported a history of knee injury, steroid therapy, steroid injections, or therapy with estrogen or bisphosphonate medications. If the patients had symptomatic bilateral knee OA, the side that was more severely affected was considered the affected side. This study was approved by our institutional review board, and all patients provided informed consent for participation in the study. Body mass index (BMI) was calculated as an index of obesity. Scores for a Knee Society rating system, which consists of a knee score and a function score, were calculated. The scores ranged from 0–100 points, with 100 being the best score. The knee score allocates points for knee pain, range of motion, and stability, with deductions for flexion contracture, extension lag, and misalignment. The pain score, in which 50 points are allotted to the knee score, is deducted with increasing frequency and severity of pain. The function score allocates points for walking distance and the ability to ascend and descend stairs, with deductions for walking aids (31). Simultaneously, knee pain after a 50-foot walk was measured using a 100-mm visual analog scale (VAS) (32).

Radiographs. Anteroposterior and lateral knee radiographs were taken with the patients in a standing position. To classify our patients, we used the Ahlbäck classification (1), which was based on JSN observed on routine weight-bearing radiographs. There were 37 women with Ahlbäck grade 0 (normal), 51 women with Ahlbäck grade 1 (narrowing of joint space), 51 women with Ahlbäck grade 2 (obliteration of joint space), and 53 women with Ahlbäck grade 3–5 (mild, moderate, and severe bone attrition, respectively). We divided the subjects into 2 groups according to JSN as observed on radiographs: a narrowing group with less than Ahlbäck grade 2 changes and an obliteration group with Ahlbäck grade 2 changes or more. In addition, according to the Kellgren/Lawrence grading system, 11 knees were grade 1, 28 knees were grade 2, 54 knees were grade 3, and 97 knees were grade 4 (33). The femorotibial angle (FTA) was defined as the lateral angle between the axes of the femoral and tibial shafts (34). Osteophyte ingrowth and JSN were graded on a scale of 0–3 on the basis of the Osteoarthritis Research Society International atlas (4). Measurements were performed at the medial and lateral condyles of the femur and tibia.

BMD measurements. We measured BMD values in L2–L4 vertebrae, the femoral neck, and knee condyles using a QDR-4500 Bone Densitometer (Hologic). The lumbar spine and femoral neck BMDs were analyzed using standard software. BMD of the knee condyles was measured using prosthetic hip scan software in analysis mode with the

patient in the supine position with the leg partially flexed at an angle of 20° and the axis of the tibia parallel to the scanning table. For the tibial condyles, 5 square regions of interest (ROIs) were marked under a line on the proximal tibia. The medial tibial condyle BMD was calculated in the 2 medial square ROIs, and the lateral tibial condyle BMD was calculated in the 2 lateral square ROIs. For the femoral condyles, 2 square ROIs of the same size as those in the tibial condyles were marked on a straight line passing through the tips of the medial and lateral condyles, with the midpoints of their distal sides at the points of contact with the respective tibial condyles. The BMD at the medial ROI was defined as the medial femoral condyle BMD and the BMD at the lateral ROI was defined as the lateral femoral condyle BMD. The ratios of the medial condyle BMD to the lateral condyle BMD (medial versus lateral condyle BMD ratio) in the femoral and tibial condyles were used as parameters for comparing BMDs at both condyles. Previous data have demonstrated that this method is reliable (25).

Statistical analysis. SPSS for Windows was used for statistical analysis. Data are expressed as means and 95% confidence intervals. Significance was set at P values less than 0.05. We used an unpaired 2-tailed t-test to determine differences in continuous variables (age, BMI, various BMD, medial versus lateral condyle BMD ratios, Knee Society knee pain scores, and VAS pain) between the narrowing and obliteration groups. In addition, we assessed the significance between the 2 groups after adjusting for age and BMI. We used partial correlation coefficients to compare 2 continuous variables (medial versus lateral condyle BMD ratios, knee condyle BMD, FTA, structural associates, Knee Society scores, and VAS pain), after adjusting for age and BMI.

RESULTS

Descriptive information. We excluded 49 men, 34 women with valgus knee OA, 45 women with hip OA, femoral neck fracture, or hemiplegia, all of which affect proximal femoral BMD, and 28 women with severe medial knee OA in whom we were unable to precisely measure radiographic angles and knee condyle BMD. Finally, a total of 192 patients were enrolled. Mean age and BMI were significantly higher in the obliteration group when compared with the narrowing group ($P < 0.001$ for age and BMI). In both the femur and the tibia, the medial condyle BMDs and medial versus lateral condyle BMD ratios were significantly higher in the obliteration group when compared with the narrowing group ($P < 0.001$ for all values), which showed a significant difference after adjusting for age and BMI. Lower knee pain and function scores and higher VAS pain were observed in the obliteration group compared with the narrowing group ($P < 0.001$ for all values). However, the mean lumbar spine BMD, which showed no differences between both groups, showed a significant difference after adjusting for age and BMI ($P < 0.001$) (Table 1).

In total, 63.5% of femoral condyles and 70.8% of tibial condyles had medial osteophyte scores of 2 or 3, whereas 22.4% of femoral condyles and 32.8% of tibial condyles had lateral osteophyte scores of 2 or 3. The lateral JSN score was 0 in 184 knees and 1 in 8 knees; none of the knees demonstrated scores of 2 or 3 (Table 2).

Association of BMDs and BMD ratios between the femoral and tibial condyles. Significant positive correlations were observed between the femoral and tibial condyles in the following parameters: medial condyle BMDs, lateral condyle BMDs, and medial versus lateral condyle BMD

Table 1. Descriptive information for joint space narrowing and obliteration groups in women with knee osteoarthritis*

	Total (n = 192)	Narrowing group (n = 88)	Obliteration group (n = 104)	P†	Adjusted P‡
Age, years	69.5 (68.2–70.8)	66.8 (64.7–68.9)	71.8 (70.4–73.2)	< 0.001	
Body mass index, kg/m^2	25.6 (25.0–26.2)	24.3 (23.5–25.1)	26.7 (25.9–27.6)	< 0.001	
Lumbar spine BMD, gm/cm^2	0.892 (0.869–0.915)	0.872 (0.836–0.907)	0.909 (0.878–0.940)	0.113	< 0.001
Femoral neck BMD, gm/cm^2	0.634 (0.617–0.650)	0.643 (0.618–0.667)	0.626 (0.603–0.649)	0.326	0.899
Medial femoral condyle BMD, gm/cm^2	1.205 (1.163–1.247)	1.026 (0.975–1.078)	1.356 (1.308–1.403)	< 0.001	< 0.001
Lateral femoral condyle BMD, gm/cm^2	0.691 (0.669–0.713)	0.712 (0.675–0.748)	0.674 (0.647–0.700)	0.098	0.811
Femoral medial vs. lateral BMD ratio	1.800 (1.727–1.874)	1.494 (1.403–1.585)	2.060 (1.974–2.145)	< 0.001	< 0.001
Medial tibial condyle BMD, gm/cm^2	0.954 (0.919–0.988)	0.815 (0.774–0.857)	1.071 (1.030–1.112)	< 0.001	< 0.001
Lateral tibial condyle BMD, gm/cm^2	0.631 (0.610–0.651)	0.659 (0.624–0.694)	0.607 (0.584–0.631)	0.016	0.541
Tibial medial vs. lateral BMD ratio	1.538 (1.479–1.599)	1.259 (1.202–1.316)	1.776 (1.701–1.850)	< 0.001	< 0.001
Knee Society knee score, points	54.2 (51.1–57.4)	70.4 (66.6–74.2)	40.5 (37.7–43.4)	< 0.001	< 0.001
Knee Society pain score, points	29.8 (28.5–31.2)	35.2 (33.2–37.3)	25.3 (23.9–26.6)	< 0.001	< 0.001
Knee Society function score, points	59.9 (56.5–63.4)	74.6 (69.6–79.5)	47.6 (44.1–51.0)	< 0.001	< 0.001
Visual analog scale pain, points	69.8 (65.9–73.7)	53.0 (47.1–59.0)	84.0 (80.7–87.2)	< 0.001	< 0.001

* Values are the mean (95% confidence interval). BMD = bone mineral density.
† By unpaired 2-tailed t-test.
‡ Adjusted for age and body mass index.